Chem Soc Rev

Porphyrinoid Actinide Complexes

Journal:	*Chemical Society Reviews*
Manuscript ID	CS-REV-02-2022-000107.R1
Article Type:	Review Article
Date Submitted by the Author:	12-Apr-2022
Complete List of Authors:	Vargas-Zuniga, Gabriela; University of Texas, Chemistry and Biochemistry Mangel, Daniel; Univ Texas Austin, Chemistry Boreen, Michael; University of California, Department of Chemistry Arnold, John; University of California, Department of Chemistry Sessler, Jonathan; Univ Texas Austin, Chemistry

SCHOLARONE™
Manuscripts

ARTICLE

Porphyrinoid Actinide Complexes

Gabriela I. Vargas-Zúñiga,[*a] Michael A. Boreen,[b] Daniel Mangel,[a] John Arnold,[*b] and Jonathan L. Sessler[*a]

The diverse coordination modes and electronic features of actinide complexes of porphyrins and related oligopyrrolic systems (referred to as "porpyrinoids") have been the subject of interest since the 1960s. Given their stability and accessibility, most work with actinides has focused on thorium and uranium. This trend is also seen in the case of porphyrinoid-based complexation studies. Nevertheless, the diversity of ligand environments provided by porphyrinoids has led to the stabilization of a number of unique complexes with the early actinides that are often without structural parallel within the broader coordination chemical lexicon. This review summarizes key examples of prophyrinoid actinide complexes reported to date, including the limited number of porphyrinoid systems involving transuranic elements. The emphasis will be on syntheis and structure; however, the electronic features and reactivity pattern of representative systems will be detailed as well. Coverage is through December of 2021.

Introduction

The rich and varied coordination chemistry of actinide porphyrin analogues (referred to generally as "porphyrinoids") has made these species of interest from the perspective of ligand design, electronic structure, and theory. Aspects of this chemistry, such as enhanced covalent interactions of the 5f shell observed in actinide element complexes, are not necessarily recapitulated in the case of ostensibly analogous 4f-element species.[1–3] More broadly, understanding the bonding in actinide porphyrinoid complexes or the nature of the coordination environment seen in such systems may help in the future design of synthetic targets that could be relevant to the nuclear industry or in the remediation of spent nuclear fuel.[4] However, actinide coordination chemistry remains challenging. The high radioactivity and toxicity of many actinides requires specialized facilities. This has limited the number of actinide porphyrinoid complexes reported to date. Nevertheless, important advances have been made in terms of both theory and experiment.

The ability of porphyrinoid macrocycles to coordinate actinide cations has been recognized since the 1960s. For example, the thorium, uranium, and neptunium phthalocyanine complexes–the last one detected by radiochemical means–were reported early on.[5–8] Pioneering studies revealed that the relatively high coordination number of the early actinides allowed stabilization of macrocyclic complexes, such as uranyl superphthalocyanine (SPcUO$_2$), based on a larger pentaaza analogue of phthalocyanine.[9–12] In the case of uranium and thorium cations, a number of unusual architectures were found to be stabilized with phthalocyanines and porphyrins that could not be accessed using transition metal cations.[5] Seminal investigations involving other actinide cations, such as protactinium and neptunium, were carried out in the 1965–1970 time frame; however, the resulting species were not extensively studied.[6,13]

The late 1980s saw the advent of so-called expanded porphyrin chemistry. As a general rule, expanded porphyrins incorporate a larger central cavity, a greater number of heterocyclic subunits, and more extensive conjugation than porphyrins or phthalocyanines. This led to an appreciation that such species, as a class, might prove to be excellent ligands for the actinide cations.[14,15] It was expected that relative to simple porphyrins, expanded porphyrins would provide ligand environments that would support the formation of complexes with both long-lived early actinide elements and selected radionuclides with shorter half-lives. Some of this promise has now been realized, but much in this area of chemistry remains to be explored. Accordingly, we believe it is appropriate to summarize accomplishments made to date with a view to highlighting opportunities for future research.

Tetrapyrrolic Porphyrinoids

Phthalocyanines

Phthalocyanines (Pcs) and their metal complexes have been intensively studied for almost a century. These macrocycles were accidentally discovered in 1928 during the industrial production of phthalimide in the Grangemouth works of

a. Department of Chemistry, The University of Texas at Austin, 105 East 24th Street, Stop A5300, Austin, Texas 78712, USA. E-mail: sessler@cm.utexas.edu
b. Department of Chemistry, University of California, Berkeley, CA 94720, USA. E-mail: arnold@berkeley.edu

Messrs Scottish Dyes, Ltd., and fully characterized by Linstead in 1934.[16,17] Pcs are 18 π-electron aromatic macrocycles that possess remarkable photophysical, chemical, thermal, and photostability. As a result, Pcs have seen wide-spread use, including as dyes, pigments,[18] catalysts,[19] sensors,[20] photovoltaic devices,[21] and probes for bio-imaging and photodynamic therapy.[22,23]

The four nitrogen donors within the central cavity of phthalocyanines make them highly effective as ligands. The majority of reported metallophthalocyanine complexes have involved transition metal cations.[24–27] While some efforts have been devoted to the study of phthalocyanine f-element complexes, only a fraction of this work has been concerned with actinide cations. In this section, we provide a brief overview of actinide-Pc coordination chemistry. Specifically, we summarise studies involving both 2:1 (phthalocyanine:actinide) double-decker and single-decker type actinide phthalocyanine complexes.

Double-decker phthalocyanine actinide complexes

In 1968, Lux and co-workers reported homoleptic double-decker phthalocyanine complexes containing thorium(IV) and uranium(IV) cations. In their first report, the thorium(IV) and uranium(IV) complexes ($ThPc_2$ (**1**) and UPc_2 (**2**)) were obtained in 43 and 38% yields, respectively, by reaction of phthalodinitrile with the corresponding actinide tetraiodide at 240 °C and followed by sublimation at 530–550 °C/10^{-5} torr.[8] Twenty-five years later, Kadish and co-workers reported the synthesis of complexes **1** and **2** via metal exchange of disodium phthalocyanine (Na_2Pc) with thorium and uranium tetrachloride, Fig. 1. This more straightforward synthetic method nevertheless suffered from low yields (6.2% and 7.4%, respectively).[28]
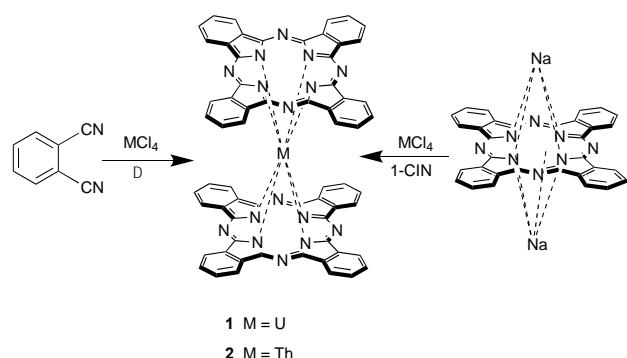

Fig. 1. Synthesis of complexes **1** and **2**. NB: 1-ClN = 1-chloronaphthalene.

In 1965, a sublimable bis(phthalocyaninato) complex of neptunium was detected by radiochemical means. This complex was apparently the first volatile neptunium complex reported; however, the complex was not isolated.[6] In 1970, Lux *et al.* reported protactinium and neptunium bis(phthalocyaninato) complexes. These complexes were prepared from the thorium and uranium complexes **2** and **1** by the elemental transformations (n,γ) (β⁻) of ^{232}Th and ^{238}U, respectively. Repeated sublimation of the irradiated parent compounds allowed the identification and isolation of the

$Pc_2^{233}Pa$ (**3**) and $Pc_2^{239}Np$ (**4**) complexes (Fig. 2), identified by the specific activities corresponding to the constituent protactinium and neptunium isotopes. These researchers also synthesized complex **4** on a trace scale (e.g., ~ 1 μg) and as a mixture of UPc_2 + $^{239}NpPc_2$ by starting from an irradiated uranium target (U + ^{239}Np) and following the standard synthesis used to obtain UPc_2.[13] In both complexes **3** and **4**, the authors proposed that oxidation state of the ^{239}Np and ^{239}Np cations is 4+.

Double-decker americium complexes were reported by Moskalev and co-workers; these species were obtained by the reaction of americium acetate with *o*-phthalonitrile followed by electrocrystallization from a dimethylformamide-hydrazine hydrate mixture.[29,30] It was suggested that the americium complex existed as $[AmPc_2]^{-1}$. However, an X-ray diffraction analysis of the crystalline powder led to the conclusion that the americium in the presumed sandwich complex (**5**) was in the tervalent state, i.e., $[Am^{III}Pc_2]^0$, in which the americium(III) centre is located between two phthalocyanine macrocycles with one acting as formal −2 charge and the other acting as formal −1 charge within each molecule(Fig. 2).

Although no further studies were conducted using complex **5**, similar bis(phthalocyaninato) complexes with lanthanide(III) ions have been studied.[31] In this report, Harnoode and co-workers analysed the EPR spectra of several neutral bis(phthalocyaninato)-Ln(III) (Ln = Eu, Sm, Gd) complexes. They noted, for example, that at −150 °C *o*-dichlorobenzene solutions of $[Eu^{III}Pc_2]^0$ exhibited a well-defined signal at *g* = 2.007, indicating the presence of an organic free radical. Therefore, it was concluded that in these neutral complexes (i.e., $[Ln^{III}Pc_2]^0$) an unpaired electron is not localized on one phthalocyanine ring but delocalized over the two phthalocyanine rings leading them to formulate the systems as $[Ln^{III}(Pc^{2-})(Pc^{-\bullet})]^0$.[31] We suggest that complex **5** has a structure similar to these bis(phthalacyaninato)-Ln(III) complexes.
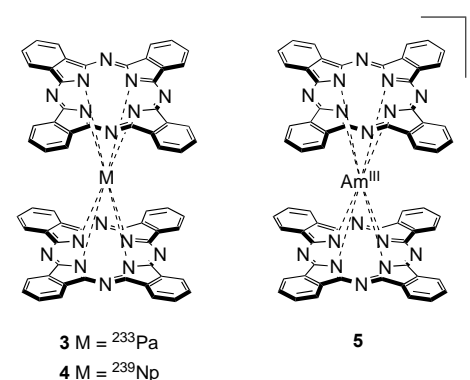

Fig. 2. Structures of the double-decker complexes **3** and **4**, and the proposed neutral radical nature of complex **5**.

Another set of interesting double-decker phthalocyanine complexes consists of the partially oxidized iodine uranium(IV) bis(phthalocyaninato) complexes ($[UPc_2]I_{5/3}$, **6**, and $[UPc_2]I_2$, **7**) reported by Janczak and co-workers (Fig. 3).[32,33] As true for other partially oxidized sandwich-type metallodiphthalocyanine complexes doped with I⁻ or Br⁻,[34–37]

the electrical properties of complexes **6** and **7** were found to depend on the number of doped atoms with the degree of doping correlated closely with the formal oxidation state of the H_2Pc macrocyclic ring.

Compound **6** was obtained by reaction of pure uranium powder with 1,2-dicyanobenzene in the presence of iodine in a 1:6:2 (w/w/w) ratio followed by pressing into pellets, which were then inserted into an evacuated ampule and heated at 200 °C for several hours.[32] Complex **7** was obtained using a slightly modified procedure wherein pure uranium powder was reacted with 1,2-dicyanobenzene under a stream of iodine in a 1:8:2 (w/w/w) ratio, and the pressed pellets were then heated at 240 °C for 4–5 h.[33] In both cases, 1,2,-dicyanobenzene underwent tetramerization to form the uranium bis(phthalocyaninato) complex wherein the iodine atoms present in the mixture served to oxidize partially the UPc_2 complex to yield black crystals of the iodine-doped product.

Although both bis(phthalocyaninato) complexes (i.e., **6** and **7**) contain a uranium(IV) atom coordinated by eight isoindole nitrogen atoms in a distorted square antiprism, some differences were noted in the corresponding crystal structures. In $[UPc_2]I_{5/3}$ (**6**), the U atom is situated between two staggered Pc rings, leading to a columnar stack of partially oxidized UPc_2 units with a formal oxidation state of the Pc ring of −1.722 (Fig. 3a). The iodine doping atoms were found within the channels between the UPc_2 units in the form of one-dimensional chains. A corresponding single-crystal X-ray analysis of complex **7** revealed quasi-one-dimensional columnar stacks of partially oxidized $[UPc_2]^{2/3+}$ units with I_3^- atoms located in the channels between the UPc_2 units as shown in Fig. 3b.[33]

Fig. 3. Packing views of the single-crystal structures of a) complex **6**, b) complex **7**, and c) model of the disorder of the iodine chains in complex **7**. Average positions (z = ¼ and equivalent positions) are shown on the left; the three orderings of the I_3^- ions are given on the right. Reprinted with permission from Refs. 30 and 31. Copyright 1999 and 2000 Elsevier.

Raman and EPR spectral analyses revealed further differences between **6** and **7**. In complex **6**, a sharp peak at ~109 cm^{-1} with an overtone progression of peaks at ~220 and ~330 cm^{-1} was seen. This led to the assignment of the iodine species as I_3^{-1}, which implied a +5/9 oxidation state per UPc_2 unit or a −1.722 formal oxidation state for the Pc ring. An overall formulation of $[UPc_2](I_3^-)_{5/9}$ was thus made.[32] This assignment is consistent with the 0.51 spins per UPc_2 molecule inferred from the EPR spectrum. In contrast, the Raman spectrum of **7** revealed that each UPc_2 unit has a +2/3 oxidation state or a −1.666 formal charge on the phthalocyanine ring thus giving a formulation of $[UPc_2](I_3^-)_{2/3}$.[33] However, integration of the single signal seen in the EPR spectrum of **7** revealed 0.15 spins per UPc_2 molecules, a value lower than that inferred from the Raman spectroscopic analysis. This discrepancy was attributed to spin-spin coupling between two monoxidized Pc^- rings within the columns.

Heteroleptic porphyrin (Por)-phthalocyanine (H_2Pc) double-decker complexes containing uranium and thorium are known. Systems with general structure MX_2Por (M = U, Th; X = Cl) were synthesized *via* the reaction of single-decker complexes with the disodium salt of phthalocyanine, Na_2Pc, by heating at reflux in 1-chloronaphthalene for 40 h. Depending on the species in question, the corresponding mixed-ligand complexes **8–13** were obtained in 20–45% yields (Fig. 4).[28] UV-visible spectral analysis of these non-symmetric M(Por)(Pc) products revealed bands attributable to each macrocycle unit, as shown in Table 1. For instance, the B band of $U(TPP)_2(Pc)$ (**9**) at 412 nm could be correlated with the corresponding B band values of $U(TPP)_2$ (402 nm) and $U(TPP)(acac)_2$ (420 nm).[38] In all cases, the sandwich complexes **8–13** exhibited characteristic absorption bands at around 480 nm, which the authors attributed to transitions involving delocalized π orbitals involving both macrocyclic moieties. Two transitions, referred to as Q' and Q'' were seen between 630–650 nm and 480–500 nm, respectively. These bands, seen in the double-decker species, were thought to result from linear combinations of transitions involving each macrocycle. The specifics were found to vary as a function of the inter-macrocycle spacing. Moreover, in the case of complex **9**, no evidence of a π−π interaction was seen, a finding ascribed to the sterically hindered TPP rings. A spectroelectrochemical analysis of $[Th(Por)(Pc)]^+$ (Por = OEP or TPP) led to the conclusion that oxidation occurs preferentially on the porphyrin ligand.[28]
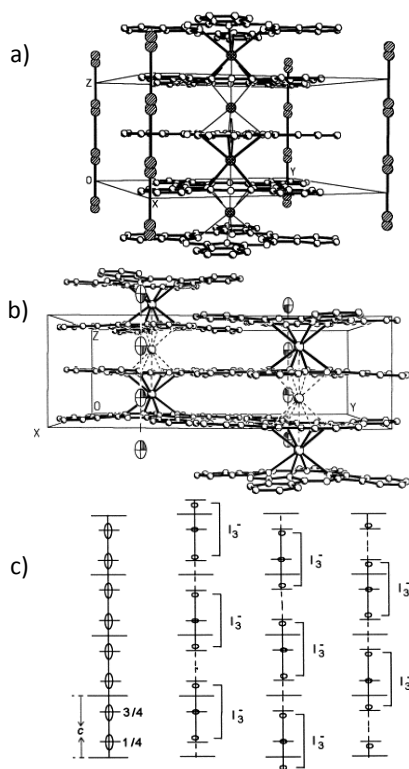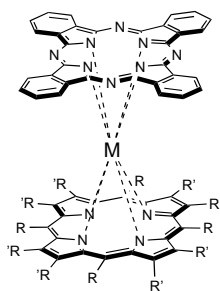
8 M = Th; R = H, R' = Et
9 M = Th; R = H, R' = Ph
10 M = Th; R = CH$_3$Ph, R' = H
11 M = U; R = H, R' = Et
12 M = U; R = H, R' = Ph
13 M = U; R = CH$_3$Ph, R' = H

Fig. 4. Structures of the heteroleptic double-decker complexes **8–13**.

Metal	Macrocycle	Compound	λ (nm)						
			H$_2$Pc	Soret band	Q'' band	Q' band			NIR
Th	H$_2$Pc	H$_2$Pc^a **2**	330 (12.4)			585 (sh)	640 (18.4)	689 (sh)	
		OEP **8**	340 (9.6)	393 (9.4)	466 (2.4)	570 (sh)	608 (2.9)		731 (0.1)
		TPP **9**	333 (6.1) 350 (sh)	412 (14.9)	479 (2.6)	575 (1.4)	624 (1.7)	700 (sh)	791 (1.5)
		TpTP **10**	330 (9.0)	412 (21.6)	480 (4.6)	577 (sh)	627 (2.3)	700 (w)	791 (2.7)
U	H$_2$Pc	H$_2$Pc^a **1**	332 (6.9)			593 (sh)	638 (9.0)	700 (2.1)	
		OEP **11**	338 (10.1)	393 (6.8)	466 (2.6)	575 (sh)	619 (3.3)		870 (0.8 br)
		TPP **12**	332 (8.5)	412 (10.3)	481 (3.7)	582 (1.6)	636 (2.3)	745 (sh)	829 (1.4)
		TpTP **13**	336 (8.6)	413 (11.0)	482 (4.2)	587 (sh)	637 (2.3)	684 (w)	827 (1.5)

Table 1. Mean (standard deviation in parenthesis) spectral data for selected homo- and heteroleptic thorium and uranium complexes in CH$_2$Cl$_2$. Adapted with permission from Ref. 28 Copyright 1993 American Chemical Society.

^{a}In pyridine. sh = shoulder; w = weak; br = broad. TpTP = tetra-*p*-tolylporphyrin

Single-decker phthalocyanine actinide complexes

In 1987, Guilard and collaborators reported the first 1:1 metal-to-phthalocyanine complexes involving uranium and thorium (**14** and **15**). These complexes, obtained as dark blue crystals in 31 and 45% yield, respectively, were synthesized from dilithium phthalocyaninate, PcLi$_2$, and acetylacetonate actinide salts (M(acac)$_4$, M = Th or U) in tetrahydrofuran (THF) at reflux (Fig. 5).[39] ^{1}H NMR spectral analyses provided support for an eight-coordinate metal ion lying outside the macrocycle plane with two acetylacetonate ligands complexed to the metal centre on the same side of the macrocycle (i.e., *cis* coordination) in analogy to what is observed in the case of single-decker porphyrin species.[38] Electrochemical studies proved consistent with redox processes that occur predominately on the H$_2$Pc ring. In addition, infrared spectra (IR) analyses revealed M–O vibration features close to 400 cm^{-1}, a finding consistent with *cis* coordination of the two acetylacetonate ligands.[39] Although the authors noted that

complexes **14** and **15** crystallized as dark blue crystals, no single-crystal X-ray diffraction data were reported.
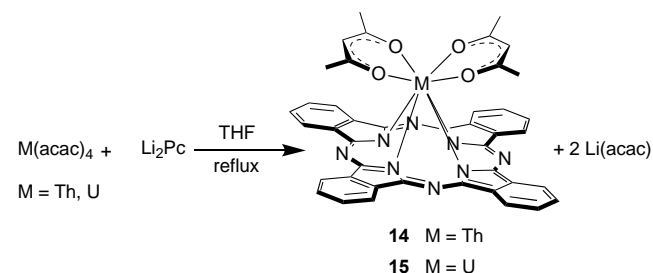

$M(acac)_4$ + Li_2Pc $\xrightarrow[\text{reflux}]{\text{THF}}$ + 2 Li(acac)

M = Th, U

14 M = Th
15 M = U

Fig. 5. Synthesis of the single-decker complexes **14** and **15**.

Despite multiple attempts to synthesize monophthalocyanine actinide complexes from the halide salts (MCl$_4$, M = Th or U), as opposed to the acetylacetonate salts, early efforts failed to produce the desired products. However, in 2020, Zhou and co-workers reported the successful synthesis of a series of

single-decker-type complexes, namely Li(THF)$_4$[PcUCl$_3$] (**16**), Na(THF)$_2$[PcU(N$_3$)$_2$Cl$_2$Li(THF)$_2$] (**17**), and the first ring-reduced (Pc^{4-}) actinide phthalocyanine complex [Li(DME)$_3$][PcUCl$_3$Li$_2$(DME)$_2$] (**18**) (Fig. 6).[40] Complex **16** was obtained in 59% yield by adding an excess of UCl$_4$ to PcLi$_2$ at 189 °C in triglyme. Treatment of compound **16** with solid NaN$_3$ in THF yielded **17** in 68% yield, whereas **18** was obtained in 39% yield by adding a strong base (KBEt$_3$H in THF) followed by dimethoxyethane (DME) into a solution of **17** in hexanes.[40]
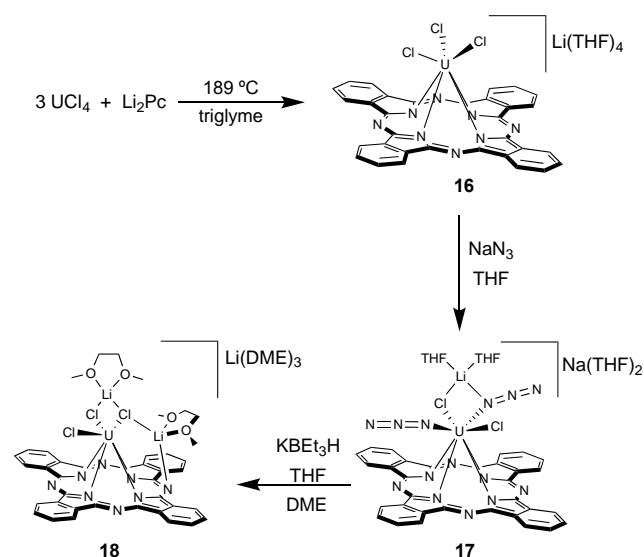

Fig. 6. Synthesis of complexes **16–18**.

A UV-Vis spectral analysis of the complexes revealed Soret- and Q-bands at 337 and 350, and 691 and 681 nm, for **16** and **17**, respectively, while the corresponding bands were seen at 328 and 545 nm in the case of the ring-reduced complex **18**.[40]

In the solid-state, the uranium(IV) centre of complex **16** is coordinated to three *cis*-bonded chloride anions. The uranium centre sits 1.425 Å above the mean H$_2$Pc plane in a capped trigonal prismatic geometry (Fig. 7a).[40] In complex **17**, the uranium(IV) centre sits even further above the mean H$_2$Pc plane (1.466 Å) and is found in an eight-coordinate square-antiprismatic geometry. In this case, one chloride and one azido ligand are bound to the uranium centre, whereas another chloride and an azide group bridge the uranium and lithium atoms. The charge of the overall anionic PcU-complex, is balanced by a sodium countercation, as shown in Fig. 7b.[40]

The reduced complex [Li(DME)$_3$][PcUCl$_3$Li$_2$(DME)$_2$] (**18**) was found to possess a seven-coordinate distorted capped trigonal

prismatic uranium centre in the solid state (Fig. 7c). The U–Cl bond lengths, 2.656, 2.763, and 2.871 Å, are similar to those of the unreduced complexes **16** and **17**. Chloride atoms serve to bridge the uranium(IV) centre to the DME-bound lithium cations. An additional outer-sphere Li$^+$ is coordinated by DME molecules. The uranium centre protrudes less far from the mean phthalocyanine-plane (1.269 Å) in the case of **18** than it does in **16** or **17**.[40] In this particular aspect, complex **18** resembles the corresponding tetraphenylporphyrin uranium(IV) analogue, where the metal cation lies 1.291 Å above the mean macrocycle plane.[41] In the case of **18**, the authors noted that the phthalocyanine core exhibited two quadrants characterized by shorter bond lengths and two quadrants with longer bond lengths (i.e., phenyl C–C distances of 1.336–1.454 Å). This pattern was also observed in the internal C–N bond lengths (i.e., 1.320–1.409 Å), which were more localized than the unreduced species (e.g., the C–N bond lengths of compound **17** are 1.349–1.370 Å).[‡][40] The bond lengths observed in compound **18** were also observed in the corresponding zirconium[42] and niobium complexes.[43] The authors attributed this partial localization to the inherent anti-aromaticity of the 20 π-electron Pc^{4-} core.
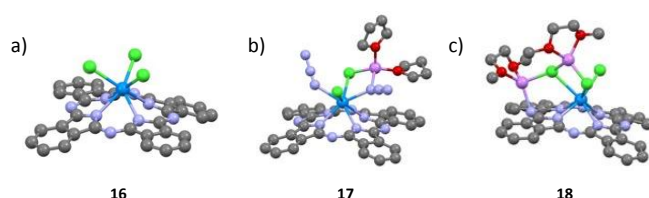

Fig. 7. Single-crystal X-ray diffraction structures of complexes **16–18**. Solvent molecules and counterions Li(THF)$_4$, Na(THF)$_2$, and Li(DME)$_3$ in a), b), and c), respectively, are omitted for clarity. This figure was generated using data downloaded from the Cambridge Crystallographic Data Centre (CSD No.1938304, 1938306, and 1938307) as originally reported in Ref. 40.

Porphyrins

Porphyrin is an 18 π-electron aromatic macrocycle that can stabilize complexes with almost every metal cation in the periodic table. As is true for phthalocyanines, metalated porphyrins have been widely studied as potential disease treatments,[44] biological imaging agents,[45] and molecular photovoltaics,[46] to name but a few of the many applications of porphyrin complexes. In contrast to transition metal and lanthanide porphyrins, actinide porphyrins have been only sparsely investigated. Most reported studies have been limited to structural and chemical characterization and the description of some chemical properties. However, as detailed below, new methods for accessing actinides are allowing actinide porphyrin complexes to be prepared that cannot be obtained by traditional synthetic techniques.

Single-decker porphyrin actinide complexes

Porphyrin-based uranium and thorium complexes have been known since the 1970s.[47] The focus on these two actinides reflects their ready availability in forms exhibiting very low radioactivity (e.g., depleted uranium).

In 1975, Wong and Horrocks reported the first porphyrin complex of an actinide element. The system in question, $(TPP)Th(acac)_2$ (**19**), was obtained in 58.8% yield by treating thorium tetra(acetylacetonate) $(Th(acac)_4)$ with tetraphenylporphyrin (H_2TPP) in trichlorobenzene (Fig. 8).[47] Complex **19**, while air-stable, was found to undergo rapid demetallation in the presence of HCl to give the protonated free ligand (H_2TPP^{2+}).[47]
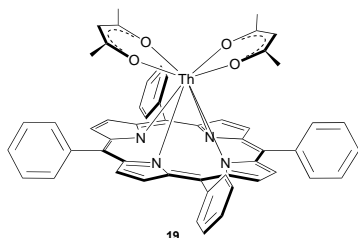

Fig. 8. Structure of complex **19**.

In 2002 Knör and Strasser reported the fluorescence and phosphorescence properties of **19**. They found that complex **19** was emissive at room temperature with a maximum at 651 nm (in toluene), a finding ascribed to intraligand fluorescence in analogy to what was seen in other transition or lanthanide metalloporphyrins.[48] For instance, the $Hf(TTP)(OAc)_2$ and ZnTPP complexes are emissive with a maximum at 633 and 645 nm, respectively.[48,49] However, the thorium complex displayed a quantum yield significantly lower ($\phi_f = 4 \times 10^{-4}$ in toluene) than the zinc tetraphenylporphyrin complex ($\phi_f = 0.033$ in toluene).[50] The authors attributed this reduction to an enhanced spin-orbit coupling induced by the coordinated thorium cation. Complex **19** also exhibited a typical porphyrin intraligand phosphoresce in degassed toluene at 298 K with a maximum at 766 nm, a finding ascribed to an efficient heavy-atom-induced population of the intraligand triplet states of the thorium complex. Support for this assignment came from the observation that the phosphorescence was quenched in the presence of molecular oxygen.[48]

An early synthesis of single-decker actinide porphyrins was reported by Dormond and co-workers in 1984; it consisted of treating MCl_4 (M = Th, U) with H_2OEP in benzonitrile (PhCN) and pyridine.[51] This afforded the corresponding $M(OEP)Cl_2 \cdot 2PhCN$ (M = Th, U) complexes **20** and **21** in 75–82% yield. Upon addition of Na(acac) in tetrahydrofuran, the respective $M(OEP)(acac)_2$ species **22** and **23** were obtained in roughly 70% yield, as shown in Figure 9.[38] The further conversion of the latter uranium complex $U(OEP)Cl_2 \cdot 2PhCN$ (**23**) to $U(OEP)Cl_2 \cdot 2THF$ (**24**) and $U(OEP)Cl_2$ (**25**) was achieved via recrystallization in a mixture of CH_2Cl_2 and THF or by heating at 200 °C under vacuum, respectively.[41]
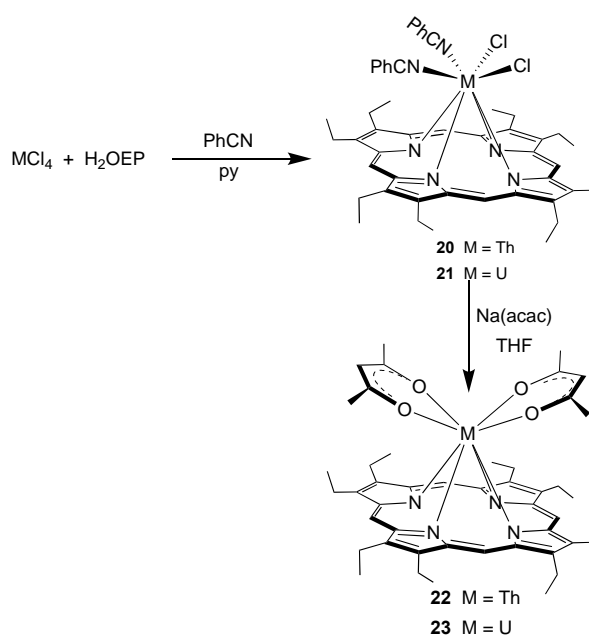

Fig. 9. Synthesis of complexes **20–23**.

^1H NMR spectroscopic analyses revealed that the diamagnetic thorium complexes **20** and **22** exhibited methylene and methyl proton signals with splitting patterns and chemical shifts consistent with a non-octahedral structure. The non-equivalence of the signals between the two sides of the porphyrin was attributed to an out-of-the-plane displacement of the metal centre with two axial ligands coordinated in a *cis* fashion. In the case of complex **22**, X-ray diffraction studies revealed an out-of-plane eight-coordinate metal centre bonded to one porphyrin macrocycle (in a convex "saucer-shaped" conformation) and two acetylacetonate ligands, as shown in Fig. 10.[38] An analogous antiprismatic coordination mode was proposed for the uranium complex $(U(OEP)(acac)_2$, **23**) in that it yielded a similar powder X-ray diffraction pattern as seen for the thorium analogue **22**.
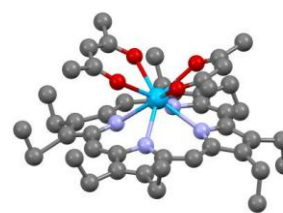

Fig. 10. Single-crystal X-ray diffraction structure of $Th(OEP)(acac)_2$ **22**. This figure was generated using data downloaded from the Cambridge Crystallographic Data Centre (CSD No. 1152765) as originally reported in Ref. 38.

In a separate study, reported in 1988, Girolami and co-workers described the synthesis of $U(TPP)Cl_2$. Recrystallization of $U(TPP)Cl_2$ from THF/1,2-dichloroethane/heptane afforded the mono-THF adduct $U(TPP)Cl_2(THF)$ (**24**), which was structurally characterized by X-ray diffraction.[41] In the solid-state, complex **32** adopts a 4:3 "piano stool" structure geometry in which the uranium lies 1.29 Å out of the mean porphyrin plane (Fig. 11). The porphyrin also adopts a slightly convex "saucer-shaped"

conformation, presumably to enhance the bonding interactions between the macrocycle nitrogen atoms and the bound metal centre.
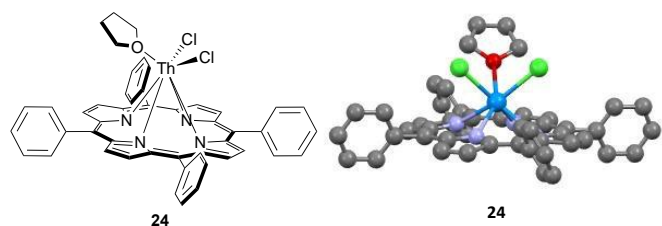

24 **24**

Fig. 11. Single crystal X-diffraction structure of U(TPP)Cl$_2$ **24**. This figure was generated using data downloaded from the Cambridge Crystallographic Data Centre (CSD No. 1153572) as originally reported in Ref. 41.

The reaction of Th(Por)Cl$_2\cdot$2PhCN (Por = TPP, OEP) with aqueous Na$_2$CO$_3$ in deoxygenated THF led to the formation of Th(Por)(OH)$_2$ in 80–82% yield depending on the choice of porphyrin.[52] These complexes were characterized by mass spectrometry as well as ^{1}H NMR and UV-vis spectroscopy, which revealed the existence of various aggregates in solution the nature of which proved dependent on the concentration of the porphyrin and the solvent. Disassociation into monomers was seen at low concentrations (*ca.* 10^{-4} and 10^{-7} M in PhCN and THF, respectively).[52] Single-crystal X-ray diffraction analyses also revealed a convex-shaped porphyrin. However, unlike compounds **22** and **24**, compound **25** is a trimeric structure [Th(TPP)(OH)$_2$]$_3\cdot$2H$_2$O in the solid-state. This trimer consists of three Th(TPP) subunits placed on each vertex of an equilateral triangle with each metal centre linked via μ-hydroxo moieties. The hydroxyl ligands, together with two water molecules, each of which is coordinated to the three thorium centres, define a trigonal prism (Fig. 12).[52] The three TPP subunits within the trimer are domed and lie parallel to the crystallographic threefold axis of symmetry. The relatively large separation between the thorium atoms (i.e., 3.960 Å) was taken as evidence of a lack of appreciable metal-metal interaction.
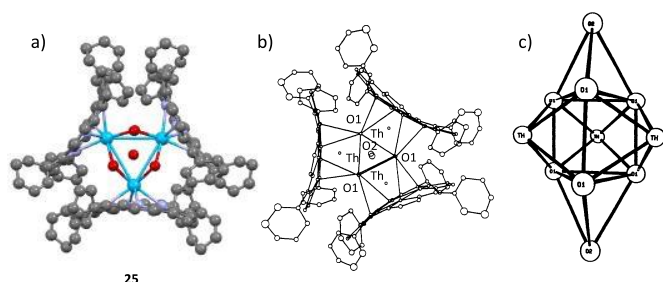

a) b) c)

25

Fig. 12. a) Single-crystal X-ray diffraction structure of the trimeric complex [Th(TPP)(OH)$_2$]$_3\cdot$2H$_2$O (**25**). This figure was generated using data downloaded from the Cambridge Crystallographic Data Centre (CSD No. 1278942) as originally reported in Ref. 52. b) Projection of the trimeric unit along the c-axis. c) ORTEP drawing of the Th$_3$(OH)$_6$(OH$_2$)$_2$ core. Reprinted with permission from Ref. 52. Copyright 1988 American Chemical Society.

Four years later, the photophysical behaviour of **25** was further examined by Tran-Thi and co-workers.[53] They found

that the fluorescence ascribed to the ^{1}(π,π*) state of the ligand in complex **25** is relatively quenched, presumably due to the presence of the heavy thorium atoms. These researchers also noted that compared to the monomer **19**, the triplet quantum yield of the trimer is drastically reduced (ϕ_X = 0.38 vs ϕ_X = 1.00). This latter finding was rationalized in terms of an enhanced probability that the singlet excited states would be deactivated via internal conversion pathways.[53]

Double-decker porphyrin actinide complexes

In 1987, Girolami and co-workers reported the synthesis of the homoleptic bis-porphyrin complex U(TPP)$_2$ **26**.[41] This metal-bridged porphyrin dimer was obtained by reaction of tetrakis(diethylamido)uranium(IV) (prepared in analogy to the thorium(IV) complex),[54] U(NEt$_2$)$_4$, with two equiv. of tetraphenylporphyrin in toluene.[41] A similar synthetic route was used to prepare the corresponding thorium(IV) analogue (i.e., Th(TPP)$_2$, **27**), as shown in Fig. 13.[55] Complexes **26** and **27** were isolated as dark purple microcrystals that exhibited Soret bands at 402 and 404 nm, respectively, in dichloromethane. These values are blue-shifted compared to what is seen for typical 1:1 metal:porphyrin complexes (λ_{max} = ca. 418 nm).[28] All features characteristic of two face-to-face porphyrins. In addition, complexes **26** and **27** exhibit less intense Q-like absorbance bands at 550 and 553 nm, for **26** and **27**, respectively. Additionally, absorption features exclusive to double-decker complexes (at 485 and 480 nm and 620 and 615 nm) were ascribed to π–π interactions within the bis-porphyrin complexes.[55,56] Cyclic voltammetric analyses revealed that both complexes undergo two chemically reversible oxidation processes near 580 and 990 mV (vs. SCE, using chloroform as solvent), respectively.[55] The authors took this redox behaviour as an indication that in both complexes the oxidations are primarily porphyrin-based.

A year later, the same research team reported the synthesis of what were stated to be the first π-radical monocation ([M(TPP)$_2$][SbCl$_6$]; M = Th, U) and π-radical dication ([M(TPP)$_2$][SbCl$_6$]$_2$; M = Th, U) actinide sandwich complexes. The oxidized compounds were obtained by reaction of M(TPP)$_2$ (M = Th, U) with phenoxathiniinylium hexachloroantimonate in dichloromethane; this afforded complexes **28** and **29** as blue-violet crystalline solids (Fig. 13).[55]

Compared with the neutral sandwich complexes **26** and **27**, the absorption spectra of complexes **28** and **29** were characterized by Soret bands that are shifted to higher energy (i.e., λ_{max} = 396 and 392 nm for **28** and **29**, respectively, in CH$_2$Cl$_2$ solution), indicative of a higher π interactions between the metal and the porphyrin π-radical cation.[55] Both complexes displayed an intense broad band centred in the near-IR region (1480 and 1270 nm, for **28** and **29**, respectively). This band was also observed in the analogous [Ce(OEP)$_2$][SbCl$_6$] (1270 nm) and initially assigned to interporphyrin charge-transfer interactions.[57] However, a detailed analysis by Bocian and co-workers of the resonance Raman spectra of Ce(Por)$_2$ and the electrochemically oxidized species, Ce(Por)$_2$$^+$ (Por = OEP or TPP), led to the conclusion that the electron-hole is delocalized over both porphyrins, implying

that this putative interporphyrin transition involves little charge transfer.[58]

EPR spectral analyses of both π-radical dication actinide sandwich complexes in frozen dichloromethane glasses at 77 K revealed the presence of two signals at g = 1.9985 and 1.9975 from **28** and **29**, a finding consistent with the proposed porphyrin-localized radical nature of these two complexes.

Although complex **28** was reported as being NMR silent in dichloromethane, the broad signals observed in the ^{1}H NMR spectrum of complex **29** recorded in deuterated dichloromethane led to the suggestion that there was some interaction between the porphyrin radical and the unpaired electrons of U(IV). Further explorations at the diamagnetic limit (infinite temperature) revealed extrapolated pyrrole signals at δ −14 ppm.[55] The authors considered this behaviour to be an indication that the porphyrin π-radical cation possesses high unpaired spin density near the pyrrole protons. This led to the conclusion that in this complex the redox processes occur near the metal centre. Despite this preliminary characterization work, no further reports regarding the presumed π-radical dications, [M(TPP)$_2$][SbCl$_6$]$_2$ (M = Th, U), have been forthcoming.
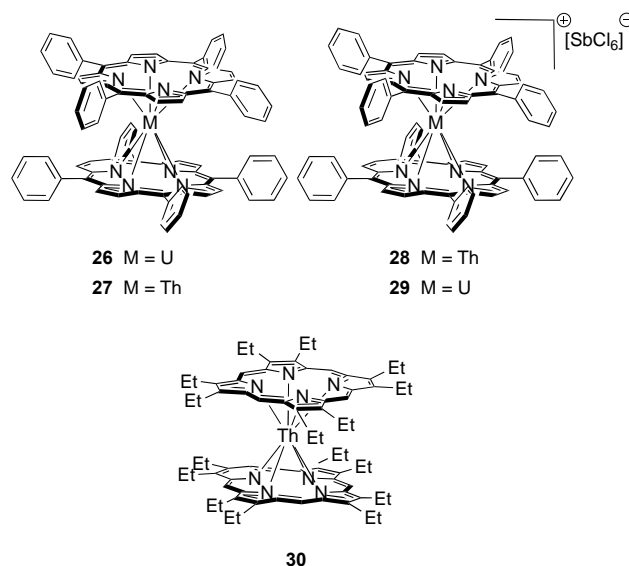

Fig. 13. Chemical structures of complexes **26**–**30**.

Single-crystal X-ray diffraction analysis of complexes **27** and **28** (Fig. 14) revealed that both the neutral and cationic complexes adopt a similar distorted square antiprismatic geometry with Th–N bond distances of 2.55 and 2.52 Å, respectively.[55] The displacement of the thorium centre from the mean plane of the porphyrin core (1.47 and 1.45 Å) mirrored what was seen in the case of the half-sandwich complex **22** (1.43 Å).[41] The two porphyrinate planes in **28** (separated by 2.89 Å) were slightly closer than in the neutral sandwich complex **27** (2.94 Å separation).[56] Nevertheless, it was suggested that the close proximity of the porphyrin planes in both complexes (i.e., **27** and **28**) allows direct electronic overlap between the two π-systems, providing additional stability to the complex. Such stabilization may also be operative in complex **30** (Th(OEP)$_2$),

where the separation between the porphyrin planes is 2.89 Å. In this case, the absence of *meso*-phenyl substituents and the associated reduction in steric repulsion was thought to allow the two porphyrin rings to adopt a staggered orientation relative to one another.
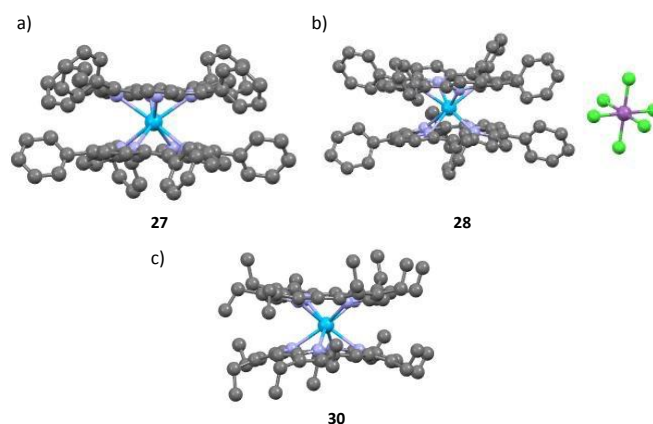

Fig. 14. X-ray crystal structures of complexes **27**, **28**, and **30**. Selected solvent molecules were omitted for clarity. This figure was generated using data downloaded from the Cambridge Crystallographic Data Centre (CSD No. 1162752, 1162754, and 1308210) as originally reported in Refs. 55 and 56.

In 2021, Rheinfrank and co-workers reported an alternative synthesis of Th(TPP)$_2$ (**27**), namely a solvent-free ultrahigh-vacuum method involving two different substrates (i.e., Ag(111) and *h*-BN/Cu(111)).[59] This in-situ synthesis consisted of three steps. First, a multilayer of the precursor H$_2$TPP was grown on the substrate of choice. This was followed by the deposition of elemental Th at room temperature and thermal annealing at 500 K for several minutes to desorb unreacted multilayer components, as shown in Fig. 15. Compound **27**, which was prepared in this way, was characterized using X-ray photoelectron spectroscopy (XPS), scanning tunnelling microscopy (STM), scanning tunnelling spectroscopy (STS), and temperature-programmed desorption (TPD). It was found that **27** was readily formed on both supports with no discernible differences (e.g., packing and molecular appearance) observed. However, a greater apparent electronic gap was seen for the sample on *h*-BN/Cu(111) with a deviation from a perfect square antiprismatic coordination geometry around the Th centre being noted in the case of **27** produced on Ag(111).[59] An advantage of the *h*-BN supported product is that it allowed for thermal desorption of the intact sandwich complex, thereby permitting further studies, such as STS. Going forward, this synthetic method may permit the preparation of new complexes containing other actinide cations whose access is limited by traditional synthetic protocols.
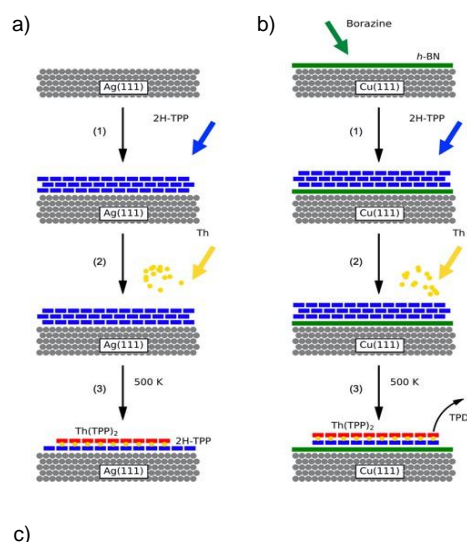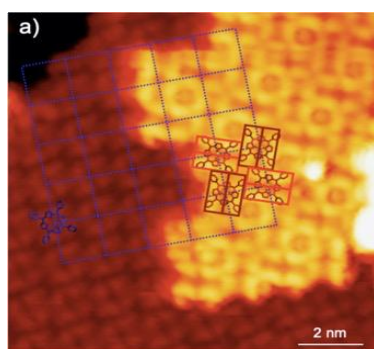
Fig. 15. a) and b) Schematic of the three-step route used to prepare Th(TPP)$_2$ on Ag(111; c) STM image of a Th(TPP)$_2$ island embedded in a 2H-TPP array. Reprinted and adapted with permission from ref. 59. Copyright 2021 American Chemical Society.

In 1993, Kadish and co-workers reported several heteroleptic bis-porphyrin complexes containing uranium and thorium (OEP)M(TPP) (M = U, Th).[28] The reaction between Li$_2$(Por) (Por = OEP, TPP) and the corresponding monoporphyrinate precursor (M(Por)$_2$Cl$_2$; M = Th, U) produced complexes **31** and **32** in 30% and 16% yield, respectively (Fig. 16). Treatment with the phenoxathiinylium radical in dichloromethane then afforded the cationic single-oxidized double-decker derivatives **33** and **34** in ca. 40% yield (Fig. 16).[28] The UV-vis spectra of the asymmetric complexes **31** and **32** exhibited characteristics seen in double-decker systems. However, the Soret and Q bands are halfway between those seen for representative symmetric diporphyrin complexes based on TPP and OEP, respectivey. For instance, the Soret band maximum of complex **31** appears at 392 nm, whereas the Soret bands of the symmetric diporphyrin complexes **27** (Th(TPP)$_2$) and **30** (Th(OEP)$_2$) are at 400 and 383 nm, respectively. Additionally, the position of the lower energy absorption features, referred to as Q'' bands (between 542–638 nm),[28] were found to depend on the spacing between the two macrocycles, which in turn reflected the specific metal centre bridging the two porphyrinate macrocycles.

Cyclic voltammetry studies in a toluene/CH$_3$CN medium revealed the generation of up to seven different oxidation states via one-electron transfer processes. In this case, the

HOMO-LUMO gaps proved comparable to what was seen in the corresponding homoleptic compounds (i.e., M(Por)$_2$; M = Th, U; Por = OEP, TPP). Therefore, this redox behaviour was taken as evidence for the presence of a single mixed orbital involving both macrocycles.
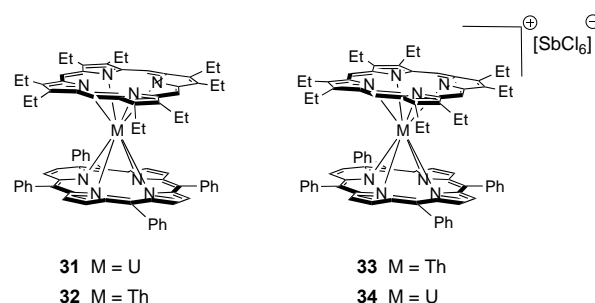

31 M = U
32 M = Th

33 M = Th
34 M = U

Fig. 16. Chemical structure of complexes **31–34**.

Triple-decker porphyrin actinide complexes

The triple-decker tetraphenylporphyrin complexes **35** and **36**, assigned as being thorium(III)[60] and uranium(III)[61] species, respectively, by Lomova and co-workers are, apparently, the only examples of triple-decker actinide complexes based on porphyrinoids.[29] The double and triple-decker uranium porphyrin complexes were prepared by heating tetraphenyl porphyrin (H$_2$TPP) and UO$_2$(AcO)$_2$ in a 1:10 molar ratio in benzonitrile or phenol at reflux for 19 h (Fig. 17). The double- and triple-decker complexes exhibited different solubilities in ethanol, which enabled the isolation of the triple-decker complexes. In the case of uranium, the double- and triple-decker complexes (**26** and **36**) formed faster in phenol than in benzonitrile. This experimental finding was rationalized in terms the phenol solvent undergoing oxidation to the corresponding quinone form with commensurate reduction of the metal cation from uranium(VI) to uranium(IV), as illustrated in Fig. 18. The authors further suggested that the transformation of the double-decker complex U(TPP)$_2$ into the triple-decker U$_2$(TPP)$_3$ proceeds in a manner analogous to what is seen in the case of multi-decker phthalocyanine complexes.[62]
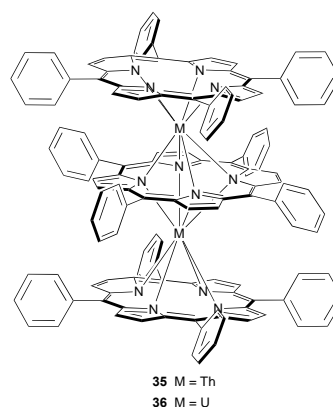

35 M = Th
36 M = U

Fig. 17. Chemical structures of the triple-decker complexes **35** and **36**.
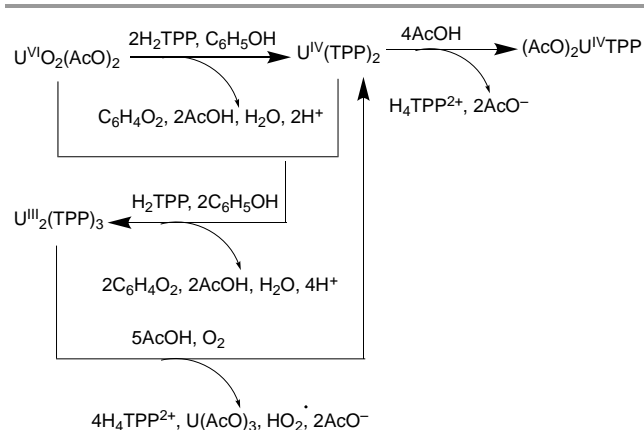
Fig. 18. Proposed reactions leading to the formation and disassociation of the triple-decker complex **36**. Adapted with permission from ref. 61. Copyright 2003 Royal Society of Chemistry.

The air-stable complexes **35** and **36** produced in this way demonstrated spectral and chemical features consistent with the expected 1:2 and 2:3 actinide:tetraphenyl porphyrin ratios. For instance, the ^{1}H NMR spectra of the triple-decker uranium(III) complex $U_2(TPP)_3$ (**36**) revealed two different peak sets corresponding to the outer and inner macrocycles. The UV-vis spectra of the triple decker complexes **35** and **36** exhibited broad bands at around 699 and 658 nm, respectively. Intense bands at 426 and 462 nm were also seen for **35** and **36**, respectively, that were attributed to a porphyrin-to-actinide(III) charge-transfer transitions.[29,61] In contrast, the broad absorption bands beyond 650 nm were ascribed to resonance interactions involving the porphyrin ligands.[29]

Dissociation of $U^{III}_2(TPP)_3$ **36** was seen upon adding 50% acetic acid (AcOH) in ethanol or benzene as deduced from UV-vis spectroscopic studies. On this basis, it was concluded that the triple-decker complex ($U^{III}_2(TPP)_3$) disassociates to give first the double-decker ($U^{IV}(TPP)_2$) complex and then the single-decker ($(AcO)_2U^{IV}(TPP)$) species, along with the free porphyrin in its protonated form (H_4TPP^{2+}) (Fig. 23). Kinetic studies, carried out in a mixture of 50% AcOH/benzene, yielded formal first-order rate constants (k^{298K}_{obs}) of 10^{-4} and 0.5×10^{-3} s^{-1} for **26** and **36**, respectively. These values reflect the higher stability of **26** relative to the corresponding triple-decker complex **36**.[61]

Corroles

Corroles are 18 π-electron aromatic tetrapyrrole macrocycles that bear considerable similarity to the porphyrins. However, corroles differ from porphyrins in several important ways. They lack one *meso*-carbon and are thus slightly contracted compared to the 20-carbon porphyrin ring.[63] Corroles also contain a trianionic nitrogen coordination core (versus the dianionic core of porphyrin). In large part due to their ability to act as trianionic ligands, corroles tend to support complexes in which the coordinated metal cation is in a higher formal oxidation state than what is typically observed in the corresponding porphyrin complexes, although the non-innocent nature of the corrole framework can lead to challenges in making oxidation state assignments.[64] Moreover,

the contracted nature of the corrole ring increases the likelihood that coordinated metal ions will sit outside of the plane of the macrocycle.[65] While less common than complexes of porphyrins and phthalocyanines, metallocorroles featuring a wide variety of metals across the periodic table have been prepared and show promise for applications including catalysis, alternative energy, biomedicine, chemical sensing, and thin film deposition.[66]

To date, only two actinide corrole complexes have been reported. The complexes in question, (Mes$_2$(*p*-OMePh)corrole)$_2$An$_2$(*μ*-Cl)$_2$(DME)$_2$ (An = Th(IV), U(IV); **37**, **38**), were synthesized by salt metathesis of the corresponding lithium corrole.[65] Specifically, treatment of (Mes$_2$(*p*-OMePh)corrole)Li$_3$·6THF with ThCl$_4$(DME)$_2$ or UCl$_4$ in DME gave **37** and **38** in 83% and 93% yield (Fig. 19).[67] While the lithium corrole is dark green, complexes **37** and **38** were isolated as dark red and dark pink crystals, respectively. Single Soret bands, were observed at 428 and 427 nm for **37** and **38** in dichloromethane. This stands in contrast to the split Soret bands seen in the corresponding free-base (407 and 428 nm) and lithium (422 and 446 nm) corroles[65] and was taken as initial evidence for a lack of planarity in the actinide complexes. Broad Q-bands were also observed at 576 and 600 for **37** and 575 and 602 nm for **38**. An absorption feature at 880 nm was observed in the U(IV) complex **38**, but not in **37**. This latter band was the tentatively assigned as an f–f transition.
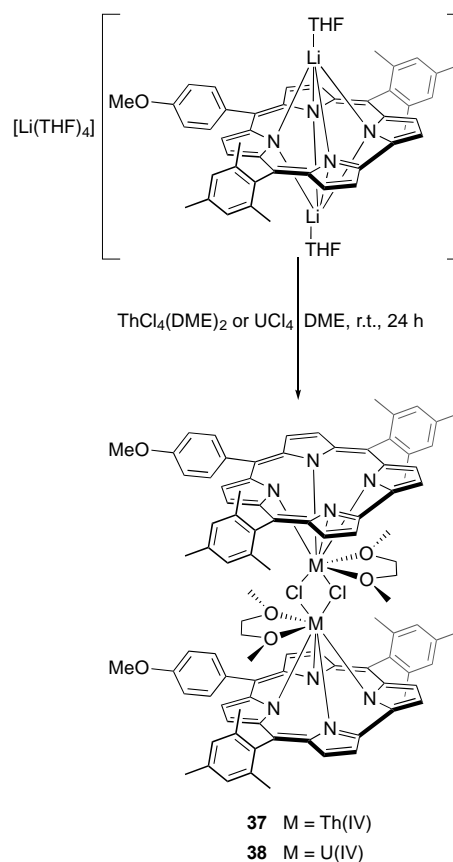

Fig. 19. Synthesis of complexes **37** and **38**.

Single crystal X-ray diffraction structural analysis of **37** and **38** confirmed loss of planarity in the corrole macrocycle and revealed a dimeric structure (Fig. 20). The Th and U centres were found to lie 1.403 and 1.330 Å out of the plane defined by the four nitrogen atoms of the corrole ligand. These values differ slightly from, but are qualitatively similar to, the corresponding values seen for the ostensibly analogous thorium and uranium porphyrin complexes for which out of plane distances of 1.424 Å and 1.29 Å were observed.[27,38] On the basis of diffusion-ordered spectroscopy (DOSY) ^{1}H NMR spectroscopic experiments, it was suggested that the dimeric structures seen for **37** and **38** in the solid state persist in solution.
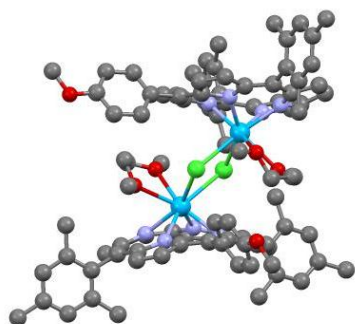

Fig. 20 X-ray crystal structure of complex **63**. The structure of **64** is isomorphic. This figure was generated using data download from the Cambridge Crystallographic Data Centre (CSD No. 930333) as originally reported in Ref. 65.

Expanded porphyrinoids

Expanded porphyrinoids (superphthalocyanines, superazaporphyrins, and expanded porphyrins) are attractive for metal coordination because they possess a larger cavity size than their tetrapyrrolic congeners. For instance, the pentapyrrolic macrocycle, sapphyrin contains a central cavity with a diameter of *ca*. 5.5 Å compared with 4.4 Å in the case of porphyrin.[68] These larger macrocycles often possess conformational flexibility and are characterized by conjugation pathways containing more than 18 π-electrons.[15] In addition, they often permit access to multiple electronic states. These features lead to differences in redox properties, as well as absorbance and fluorescence emission bands that fall into the red or even near-infrared portion of the visible spectrum.[14,69–71] Additional donor groups provide greater stability to larger metal cations and the relatively facile amine-imine conversion of the pyrrole subunits support a variety of metal coordination modes.[14,69–72] This has made expanded porphyrinoids of considerable interest in recent years. We note that key aspects of expanded porphyrin chemistry, including synthetic methods, aromaticity, coordination chemistry, and various spectroscopic features have been previously reviewed in detailed by Prof. Osuka and collaborators. We encourage the reader to consult these reviews.[69–71] Nevertheless, the actinide complexation chemistry of expanded porphyrins remains relatively unexplored.

Superphthalocyanines

The first synthesis of superphthalocyanine (SPc) coordinating a uranyl cation, SPcUO$_2$ (**39**), was reported in 1964 by Bloor *et al.* using dimethylformamide (DMF) as the solvent.[5] This ring-expanded congener of phthalocyanine, **39**, comprises five isoindole units with a uranyl ion (UO$_2^{2+}$), serving as a synthetic template and remaining coordinated within the central cavity. The uranyl cation favours a pentagonal or hexagonal planar coordination environment. Thus, its use presumably leads to the condensation of five phthalonitriles, as opposed to the four seen with most transition metal cation templates (leading to metallophthalocyanines). Notwithstanding this hindsight analysis, at the time of the original synthesis, it was assumed that the blue-black crystalline material formed in the presence of the uranyl cation was a normal uranyl phthalocyanine containing only four isoindole subunits.

In 1975, Marks, Day, and co-workers re-examined Bloor's data. They reported more detailed spectroscopic (UV-Vis, IR, and NMR)[9,10,12] analyses and concluded that five-dicyanobenzene subunits combined to yield the final uranyl-containing complex, SPcUO$_2$. Compared to normal phthalocyanines, which exhibit Q-band transitions at 665 and 698 nm (e.g., for H$_2$Pc),[11] SPcUO$_2$ exhibited two intense Q-band transitions at 810 and 914 nm. The lower energy shift observed was explained as a loss of degeneracy in the LUMO due to a lowering of the molecular symmetry from D_{5h}. A single-crystal X-ray diffraction analysis revealed five cyclized phthalonitrile units with a uranyl ion coordinated within the central cavity and corroborated the loss of molecular symmetry (Fig. 21). The macrocycle was seen to be severely and irregularly buckled. The seven-coordinate uranium cation adopts pentagonal bipyramidal geometry with U–N bond lengths of ~2.55 Å.[12] SPcUO$_2$ proved sparingly soluble in aromatic solvents. However, an NMR spectroscopic analysis could be carried out in deuterated benzene. Based on the symmetry of the resulting spectra, it was concluded that the distortion from planarity observed in the solid-state was retained in solution.[10]

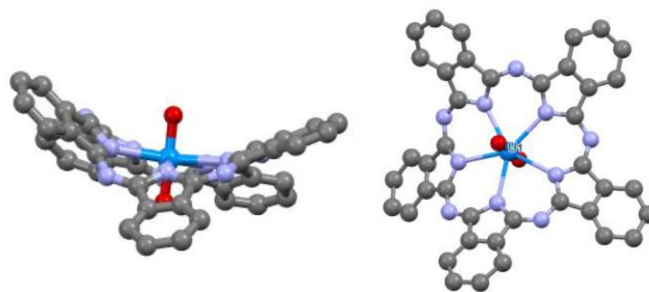**Fig. 21.** Crystal structure of SPcUO$_2$ **39** (top and side views). This figure was generated using data downloaded from the Cambridge Crystallographic Data Centre (CSD No. 1125690), as originally reported in Ref. 5.

The condensation reaction of isoindole and uranyl chloride (UO$_2$Cl$_2$) leading to the formation of SPcUO$_2$ (**39**) is accompanied by the formation of the metal-free four-member

phthalocyanine macrocycle H$_2$Pc (Fig. 22). The solvent used, DMF, was found to play a crucial role in the generation of the H$_2$Pc by-product: When the synthesis was carried out in DMF-d_7, it was found that the solvent was a source of deuterium atoms incorporated into D$_2$Pc.[10,17] Furthermore, DMF promoted tetramerization at higher temperatures (240 °C), leading to the conclusion that the SPcUO$_2$: H$_2$Pc ratio depends on the reaction conditions (i.e., temperature and the presence of water in the reagents or solvents used in the reaction).

The authors ascribed the conversion of **39** to H$_2$Pc to the action of DMF or its decomposition products (CO and HN(CH$_3$)$_2$) at high temperatures that act as scavengers for the chloride anions of the uranyl salt.[17] The HCl formed from these anions was then thought to promote the demetallation of SPcUO$_2$ leading to ring contraction and production of H$_2$Pc. The isolation of only H$_2$Pc with no evidence of the halogenated H$_2$PcCl or unreacted phthalonitrile was taken as support for this mechanistic rationale.[10] An alternative mechanism, involving a free-radical chain mediated mechanism wherein the halogen atoms serve as a radical scavenger, was considered. However, attempts at initiation with dibenzoyl peroxide or azobisisobutyronitrile were unsuccessful. Therefore, the rapid colour change observed during the reaction leading to SPcUO$_2$ (**39**) may reflect the final ring closure.

Fig. 22. Synthesis of superphthalocyanine SPcUO$_2$ **39** using as template uranyl cation (UO$_2^{2+}) and its contraction to phthalocyanine PcH$_2$ in acidic conditions.

The choice of uranyl salt employed affected the yield of the SPcUO$_2$ complex. For instance, the use of anhydrous uranyl acetate (UO$_2$(CH$_3$CO$_2$)$_2$) or uranyl nitrate (UO$_2$(NO$_3$)$_2$), instead of uranyl chloride (UO$_2$Cl$_2$), resulted in the formation of only traces of the uranyl superphthalocyanine **39**. The choice of solvent also proved to be important. For instance, DMF, in which UO$_2$Cl$_2$ is appreciable soluble, gave the highest yields.[10]

Efforts were made to prepare more soluble superphthalocyanines. Initially, the pentamethyl superphthalocyanine (Me$_5$SPcUO$_2$, **40**) was targeted. However, this analogue was obtained in a lower yield than **39** and as a mixture of isomers. In 1981 Cuellar and co-workers reported the synthesis of the uranyl decaalkylsuperphthalocyanines **40**–**42** (Fig. 23).[11] Similar to what was seen in the case of SPcUO$_2$, a shift of the visible absorption bands to lower energy was observed that proved proportional to the nature and degree of alkyl substitution (i.e., 922, 935, 939, and 938 nm for **39**, **40**, **41**, and **42**, respectively).[10]
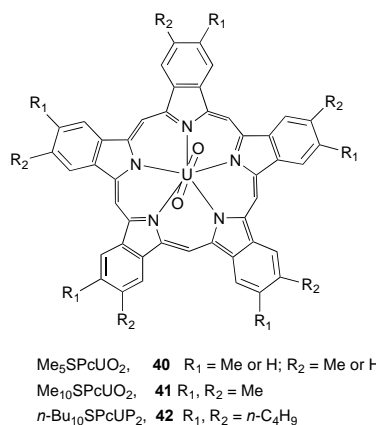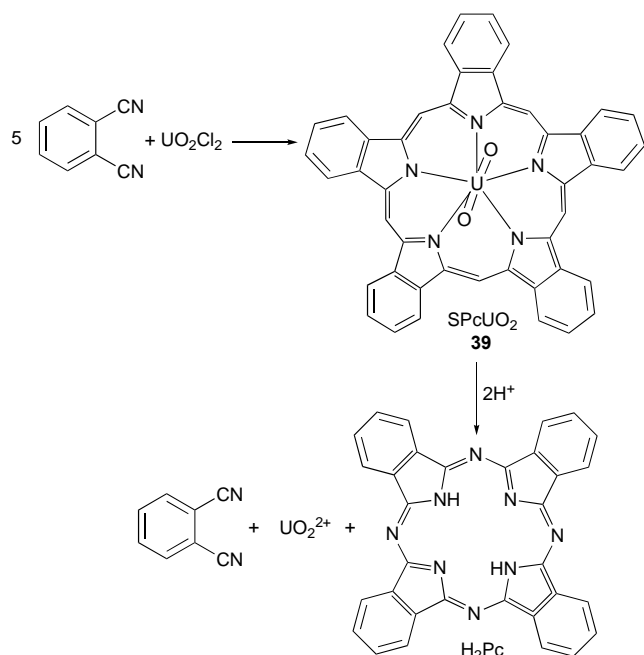

Me$_5$SPcUO$_2$, **40** R$_1$ = Me or H; R$_2$ = Me or H
Me$_{10}$SPcUO$_2$, **41** R$_1$, R$_2$ = Me
n-Bu$_{10}$SPcUP$_2$, **42** R$_1$, R$_2$ = n-C$_4$H$_9$

Fig. 23. Structure of alkyl substituted superphthalocyanines **40–42**.

Further attempts to synthesize metal-free superphthalocyanines were made, albeit without success. For instance, reaction of **39** with mineral acids (HCl) or organic acids (trichloroacetic or trifluoroacetic acid) resulted in the demetallation of the superphthalocyanine and contraction to give H$_2$Pc. Attempts to replace the uranyl ion with transition metal cations (e.g., CuCl$_2$, CoCl$_2$, ZnCl$_2$, SnCl$_2$, and PbCl$_2$ in DMF)[10] produced only the corresponding phthalocyanine complex. Reactions using other actinide salts, such as ThCl$_4$ in DMF, likewise caused decomposition of the SPcUO$_2$ complex, albeit without evident formation of PcH$_2$.[10]

Since the first reports more than 50 years ago, superphthalocyanines have been little studied, with the last report of which we are aware appearing in 1981.[9–12] Nevertheless, the SPcs remain of interest in that they possess Q bands in the near-IR region (i.e., beyond 900 nm). However, an open question is whether the original superphthalocyanine chemistry can be extended beyond the uranyl cation to include, possibly, related neptunyl or plutonyl species.

Superazaporphyrins

In 2012, Furuyama and co-workers reported the synthesis of the uranyl superazaporphyrin complexes **43–46** prepared via uranium-templated cyclization reactions.[73] The superazaporphyrin macrocycles **43–45**, shown in Fig. 24, contain five potential donor atoms derived from pyrrole subunits, or pyrrole and isoindoline in the case of the low-symmetry analogue **46** (Fig. 24), connected by five *meso*-nitrogen atoms. All four uranyl complexes were isolated as air-

stable powders; however, crystals suitable for X-ray diffraction analysis were only obtained in the case of complex **44**.
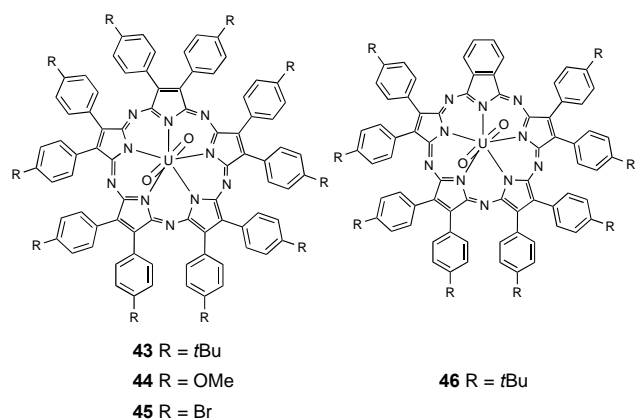

43 R = *t*Bu
44 R = OMe
45 R = Br
46 R = *t*Bu

Fig. 24. Chemical structures of superazaporphyrins **43–46**.

X-ray crystallographic analysis of **44** revealed that the uranyl cation sits in the centre of the mean pentaaza plane, as shown in Figure 25, with consequence that the macrocycle adopts a highly saddled conformation analogous to what was seen in the case of SPcUO₂. The aryl substituents lie perpendicular to the mean macrocycle plane.[73]
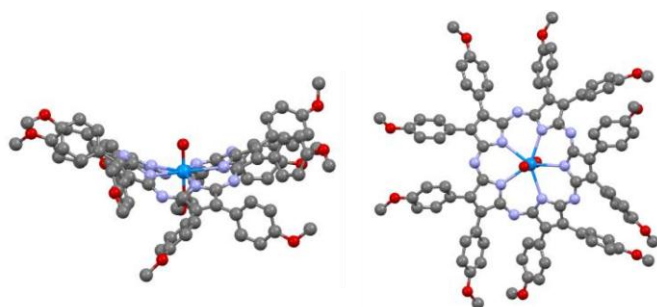

Fig. 25. Top and side views of the single-crystal X-ray diffraction structure of **44**. Solvent molecules are omitted for clarity. This figure was generated using data downloaded from the Cambridge Crystallographic Data Centre (CSD No. 876819) as originally reported in Ref. 73.

The uranyl pentapyrrolic compounds **43–45** exhibited Q-like absorption bands beyond 800 nm. It was found that the pyrrolic substituents only affected the position of the Q-type bands modestly (λ = 878, 871, and 845 nm for **43**, **44**, **45**, respectively), in chloroform.[73] Compared to **39**, the Q-like band of the superazaporphyrins were shifted to shorter wavelength ($\Delta\lambda \leq 37$ nm). This shift resembles the difference in the Q-bands seen between phthalocyanine (λ = 675 nm)[74] and octaaryltetraazaporphyrin (λ = 635 nm) in chloroform.[75] In contrast, a Q-like band is seen at 884 nm in the case of the low-symmetry complex **46**, leading to the suggestion that **46** displays features intermediate between those of **43** (λ = 878 nm) and uranyl superphthalocyanine **39** (λ = 915 nm). In analogy to what was seen for this latter complex, attempts to remove the UO_2^{2+} cation from the superazaporphyrins or exchange the coordinated uranyl centre with other common cations (e.g., Ni(II), Zn(II), Cu(II), or Lu(III)) resulted in decomposition.

Pentaphyrins

Expanded porphyrins containing five heterocyclic rings, known as pentaphyrins, generally contain a formal 22 π-electron periphery. The specific electronic distribution differs, however, depending on the bridging carbons linking each heterocyclic unit. Pentaphyrins, as a class, are among the oldest known porphyrinoids. Their preparation early on was made possible by modifying such classic porphyrin synthetic methodologies as the MacDonald and Rothemund acid-catalysed condensations.[14,76] Nevertheless, as detailed below, their actinide coordination chemistry remains limited with the complexes successfully obtained and structurally characterized involving mostly the uranyl cation and a limited subset of the known pentaphyrins.

Pentaphyrin(1.1.1.1.1)

The expanded porphyrin [22]-pentaphyrin(1.1.1.1.1), prepared by Rexhausen and co-workers in 1983,[77] is a pentapyrrolic macrocycle containing five *meso*-carbon bridges. Burrell and co-workers reported the first structurally characterized UO_2^{2+} coordination complex with an expanded porphyrin using this pentapyrrolic macrocycle as a ligand almost a decade later.[78] The decaalkyl pentaphyrin uranyl complex **47**, Fig. 26a, was obtained as a dark green solid by reaction of the triprotonated form with UO_2Cl_2 in a 1:1 v/v solution of pyridine and 2-propanol under reflux conditions. Complex formation was monitored by UV-vis spectroscopy until a single B-like band at 500 nm was observed.[78] The absence of pyrrolic NH signals in the ¹H NMR spectrum was taken as further evidence for the coordination of the uranyl cation within the macrocyclic cavity. More definitive evidence came from a single-crystal X-ray diffraction analysis of **47**, which revealed a uranyl cation pentacoordinated within the centre of the macrocycle. As shown in Fig. 26b, the macrocycle was found distorted from planarity in a saddle-like manner. The distortion from planarity was ascribed to the presence of the uranyl cation in a pentagonal bipyramidal coordination geometry and a slight size mismatch between the cation and the ligand.[72,78]

In marked contrast to what was observed for the uranyl superphthalocyanine (**39**), the uranylpentaphyrin complex **47** was soluble in all common organic solvents, relatively resistant to hydrolysis, and stable in the presence of other metal salts. It was also noted that, unlike **39**, complex **47** did not undergo appreciable decomposition under strongly acidic conditions. Therefore, once prepared, the metal could be removed from complex **47** via protonation to regenerate the metal-free ligand.
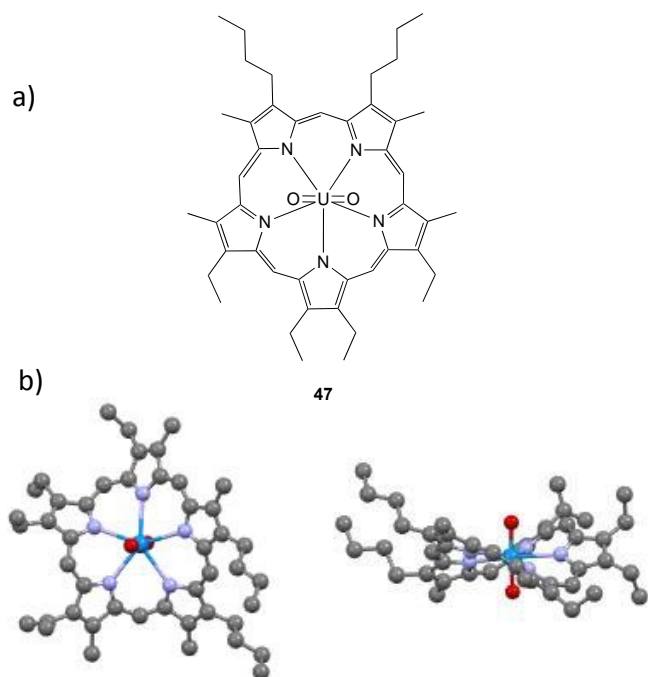
Fig. 26. A) Chemical structure of the pentaphyrin uranyl complex **47**. B) Top and side views of the X-ray crystal structure of complex **47**. This figure was generated using data downloaded from the Cambridge Crystallographic Data Centre (CSD No. 1285033) as originally reported in Ref. 78.

In 2002, Sessler and co-workers, in collaboration with Keogh at Los Alamos National Laboratory, reported the synthesis of the neptunyl (NpO$_2^{2+}$) and plutonyl (PuO$_2^{2+}$) pentaphyrin complexes. The compounds were characterized by UV-vis and ^{1}H NMR spectroscopy. However, no crystal structure was obtained for either of these putative transuranic complexes.[79]

Sapphyrin and oxasapphyrin

The serendipitous synthesis of [22]-pentaphyrin(1.1.1.1.0) by Woodward in 1966—called sapphyrin for its bright blue colour—motivated investigations into is presumed actinide coordination chemistry.[80] Although members of the Woodward research group predicted that this aromatic 22 π-electron macrocycle would favour a pentagonal coordination geometry and thus likely accommodate a uranyl cation within its pentaaza core, no uranyl complex was isolated.[68] Years later, Sessler and co-workers reported the synthesis of the uranyl complex **48** obtained from the reaction of sapphyrin and UO$_2$Cl$_2$ in the presence of pyridine and trimethylamine in methanol. Although a number of other reaction conditions were tested in an effort to obtain the expected aromatic sapphyrin-uranyl complex, in fact what was isolated was a non-aromatic complex wherein a methoxy group had added to one of the *meso*-like bridging positions (Fig. 27a).[81] A single-crystal X-ray diffraction analysis of this uranyl complex (**48**) confirmed the structural assignment (Fig. 27b).[81] The authors speculated that this addition could reflect activation of a methanol molecule by the uranyl cation. This methane bridge rehybridization (from sp^2 to sp^3, via formal nucleophilic addition of a methoxide anion) results in dearomatization of the ligand. It was thus an early example of a change in

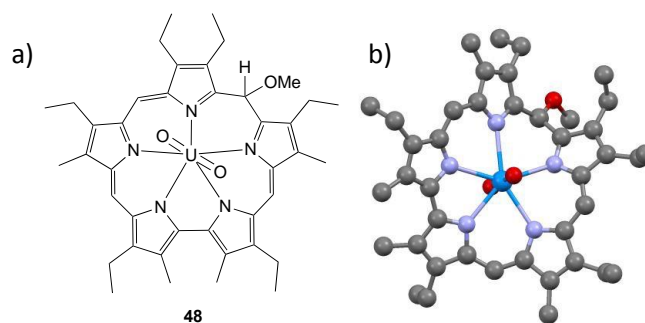electronic structure induced by actinide cation coordination, a theme that remains of interest to this day.[81]

Fig. 27. A) Chemical structure of the pentaphyrin uranyl complex **48**. B) X-ray crystal structure of complex **48**. This figure was generated using data downloaded from the Cambridge Crystallographic Data Centre (CSD No.1188695) as originally reported in Ref. 81.

The same research group later reported a sapphyrin-like derivative containing oxygen, termed monoxasapphyrin. The uranyl complex (**49**) was obtained as a green solid by heating uranyl diacetate with monoxasapphyrin in acetonitrile and triethylamine (Fig. 28a).[82] In contrast to what was observed in the case of sapphyrin, uranyl cation complexation did not lead to attack on the macrocyclic core, which remained aromatic upon coordination. The UV-vis spectrum of **49** resembled the one observed for sapphyrin with a strong Soret band at 454 nm and three weaker Q-like bands at 625, 633, and 689 nm, respectively.[82] A single-crystal X-ray crystallographic analysis revealed a twisted ligand with the uranyl cation residing within the mean plane, as shown in Fig. 28b. [82] However, the uranyl in **49** was not situated in the centre of the oxasapphyrin, but more towards the pyrrolic nitrogen atoms. Indeed, it was found that the U–O distance in **49** was larger (2.791 Å) than the corresponding U–N distances (2.449–2.587 Å). Furthermore, the saddle-shaped conformation of the macrocycle was less pronounced than, for example, in the pentaphyrin complex **47**.

Although the authors did not provide an explanation for the disparate reaction products obtained with sapphyrin and oxasapphyrin, it is likely that substitution of a N atom for an O atom in oxasapphyrin leads to a decrease in the average cavity size. Therefore, the uranyl cation fits better into the cavity than it would in the corresponding putative uranyl sapphyrin complex. This size matching is expected to allow for more effective electron overlap between the uranyl centre and the pyrrolic nitrogen atoms leading to a more stable complex. A reduction in the cavity size likely also accompanies rehybridization of the *meso*-carbon bridge in the case of **48**. Although aromaticity is lost, any decrease in electronic stabilization energy is presumably compensated for by a strengthening of the metal-nitrogen bonds that results from the decrease in macrocycle ring size. A better charge match—sapphyrin is a formal trianionic ligand, whereas oxasapphyrin is a formal dianionic ligand—likely also contributes to the different outcomes seen for these ostensibly similar macrocycles when allowed to react with the uranyl cation. As

ARTICLE

discussed in the section entitled Theoretical predictions and comparisons of porphyrinoid actinide complexes, the seemingly unusual reactivity seen for sapphyrin has been the subject of theoretical studies.
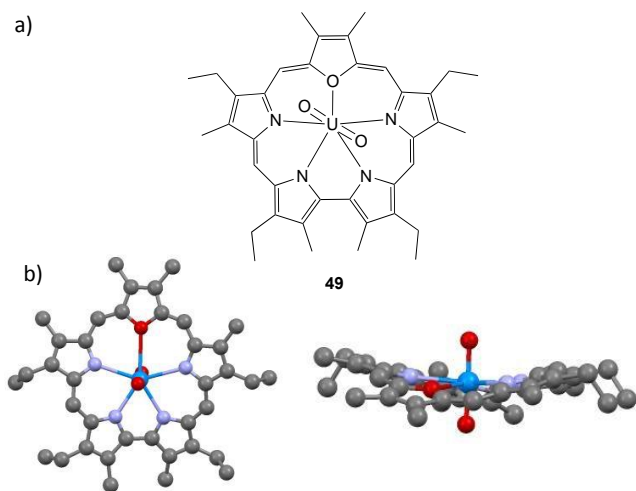

Fig. 28. A) Chemical structure of complex **49**. B) Top and side views of the X-ray crystal structure of complex **49**. This figure was generated using data downloaded from the Cambridge Crystallographic Data Centre (CSD No. 1187239) as originally reported in Ref. 82.

Hexaphyrins

Hexaphyrins are expanded porphyrins that contain six heterocyclic units linked by six, four, or even fewer methane bridges. Many have historical names, such as rubyrin,[83] rosarin,[84] amethyrin,[83,85] and isoamethyrin.[86] Several of these systems have been studied extensively as ligands for transition metal cations. In contrast and in spite of their containing six potential pyrrole nitrogen donor sites, reported actinide complexes of hexaphyrin-type expanded porphyrins are limited in number, being known only for amethyrin, isoamethyrin, pyrihexaphyrin, and dipyrihexaphyrin.

In the case of amethyrin, isoamethyrin, pyriamethryin, and dipyriamethyrin ⎯all containing *meso*-carbon bridges⎯ the macrocyclic core of these macrocycles was found to adopt a more pronounced saddle-shaped conformation when coordinated to the uranyl cation than the pentapyrrolic compounds presented above. This greater distortion from planarity, and associated closing up of the internal cavity, is believed to allow a better fit to the metal centre, resulting in more stable complexes.[69,70,72,87] It is worth noting that the majority of these macrocycles contain alkyl substituents on the β-positions of the pyrrole units, which may also contribute to steric effects that prevent a more planar conformation.[87]

Amethyrin and isoamethyrin

In 1995, Sessler and co-workers reported the synthesis of a 24 π-electron system they named amethyrin ([24]hexaphyrin(1.0.0.1.0.0)) for its characteristic purple colour in its reduced form.[83] In this first report, a description of a presumed uranyl (UO_2^{2+}) complex (**50**) with this macrocycle was provided (Fig. 29).[83] The synthesis involved the use of

$UO_2Cl_2 \cdot 3H_2O$ and triethylamine in absolute methanol and produced complex **50** 63% yield. Twenty-three years later it was found that the use of drier conditions (anhydrous THF and $UO_2[N(SiMe_3)_2]_2$) provided a higher yield (83%).[88] Although initial UV-vis spectroscopic and mass spectrometric analyses,[83] followed by a more detailed characterization in 2018,[15,88] proved consistent with the existence of complex **50**, no structural data was reported. However, a ^1H NMR spectroscopic analysis revealed the absence of pyrrole NH protons, which was taken as evidence of the formation of an oxidized dianionic ligand coordinating the uranyl cation via all six nitrogen atoms provided by the amethyrin ligand core.[88]

In 2002, Sessler, Keogh, and co-workers explored the coordination chemistry of amethyrin with other actinyl cations.[79] In the case of the neptunyl (NpO_2^+) cation, complex **51** was obtained as a red microcrystalline solid, which was characterized by UV-vis, NMR, and Raman spectroscopies. Although characterization of **51** was limited due to the highly radioactive nature of the complex, a signature band was identified in the absorption spectrum at 977 nm corresponding to the NpO_2^+ cation.[79] This led to the conclusion that spontaneous ligand oxidation and neptunium reduction (from Np(VI) to Np(V)) occurred upon metal cation coordination. Follow-up ^1H NMR spectroscopic analysis of the N–H resonances led to the suggestion that neptunyl coordination occurs on one side of the cavity to produce a so-called sitting atop complex. Unfortunately, no crystal structure data was reported that could serve to confirm or refute this suggestion. In a later report detailing the characterization of the uranyl complex **50**, it was suggested that the neptunyl cation is hexacoordinated to the macrocycle (Fig. 29).[88] However, in the absence of structural data it remains an open question whether coordination of the neptunyl cation to amethyrin-type ligands occurs preferentially on one side——as initially suggested in the context of studies involving **51**—— or involves a hexacoordinated ligation mode as later proposed.
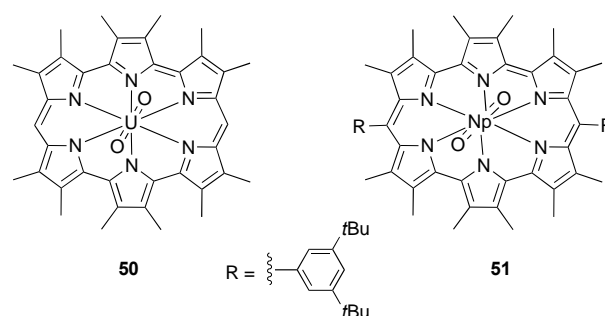

Fig. 29. Chemical structure of complex **50** and one proposed structure for complex **51**.

A related macrocycle [24]hexaphyrin(1.0.1.0.0.0), termed isoamethyrin, was reported by the same research team.[86] It proved to be an effective ligand for high-valent actinyl cations (i.e., UO_2^{2+}, NpO_2^+, and PuO_2^+; **52–54**) as shown in Fig. 30a.[79,86] In all cases, a dramatic colour change from yellow to bright pink was observed upon exposure to the actinyl salt (i.e., $UO_2(OAc)_2 \cdot 2H_2O$,[86] an incompletely characterized mixture of NpO_2Cl_2[79] and NpO_2Cl,[86] or PuO_2Cl_2[79]) in protic media. The

coordination of Np(V) and Pu(V) produced an immediate colour change, whereas a gradual colour change was observed upon the insertion of the U(VI) cation. These colour changes were ascribed to oxidation of the macrocycle from a 4n π-electron form to a formally aromatic 4n+2 π-electron species upon the metal cation complexation. This conversion was faster in the case of metal salts with lower redox potentials (i.e., NpO_2^+, and PuO_2^+; giving complexes **53** and **54**). Both complexes **52** and **53** yielded crystals suitable for single-crystal X-ray diffraction analysis. In each case, the actinyl cation was found to sit within the macrocycle cavity in a distorted hexagonal bipyramidal coordination geometry, as shown in Fig. 30b.[86]
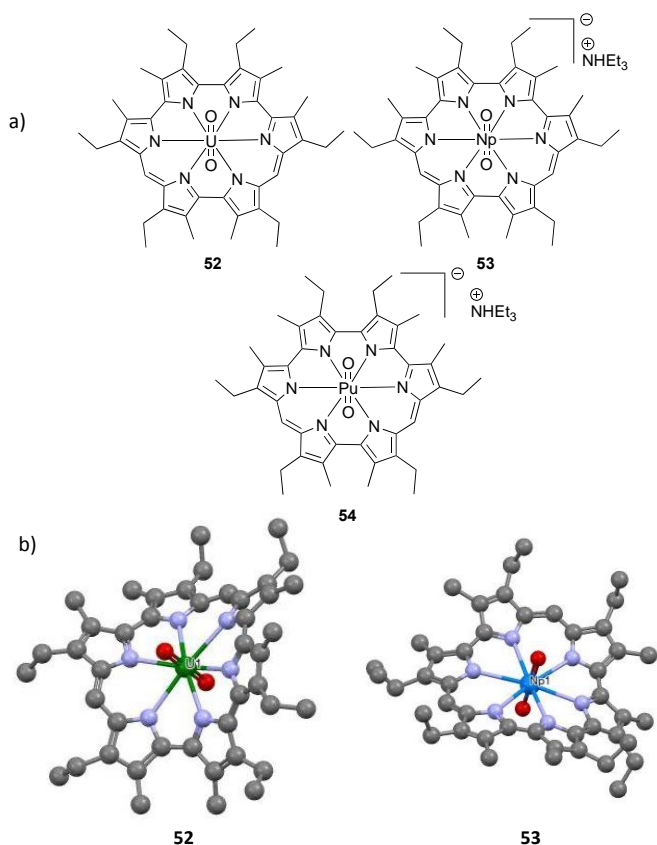

Fig. 30. A) Chemical structures of complexes **52–54**. B) X-ray crystal structures of the uranyl and neptunyl complexes **52** and **53**. Solvent molecules were omitted for clarity. This figure was generated using data downloaded from the Cambridge Crystallographic Data Centre (CSD No.149932 and 150148) as originally reported in Ref. 89.

The radioactive nature of complexes **53** and **54**, which require specialized infrastructure and work on small scale, limited further studies. However, isoamethyrin was investigated as a potential colorimetric sensor for the uranyl cation. The yellow-to-pink colour change that accompanied uranyl cation complexation allowed detection of the uranyl cation with a limit of detection of ca. 28 ppb in a mixed solvent system consisting of methanol-dichloromethane (9:5, v/v).[86] In further studies, a matrix-supported system containing isoamethyrin was designed for the determination of U(VI) concentration. Unfortunately, the colorimetric response (> 1 day) proved too

slow for practical use. Subsequently, isoamethyrin was introduced into a fibre optic system that exhibited selectivity for the uranyl cation over typical interferants while providing a detection limit in aqueous media of ≤100 ppb.[86]

The isoamethyrin derivative naphthoisoamethyrin, containing the π-extended moiety, naphthobipyrrole, was synthesized to confer rigidity to the macrocycle (Fig. 31a).[89] This particular macrocycle, prepared under acid-catalysed MacDonald conditions, exhibited a broad absorption at 610 nm in chloroform, which contrasts with the characteristic absorbance bands at *ca.* 580 nm seen for isoamethyrin.[86] This difference in the UV-vis spectrum was attributed to the relatively more rigid structure for naphthoisoamethyrin, an inference supported by X-ray single crystal diffraction.[89] On this basis, it was inferred that actinide cation coordination would not induce an appreciable distortion of the macrocyclic ring.

This structural prediction proved to be true in the case of complex **55**. This metalated derivative was obtained by reaction of naphthoisoamethyrin with a uranyl silylamide salt, $UO_2[N(SiMe_3)_2]_2$ (Fig. 31).[89] This bench stable complex features a Soret-like band at 514 nm in chloroform and an additional Q-type absorption at 813 nm. These spectral features were interpreted as evidence of a two-electron oxidation occurring during metal insertion to yield an aromatic chromophore. This inference was supported by cyclic voltammetry studies in dichloromethane that revealed reversible redox events attributed to a 22 π-aromatic system. A single-crystal X-ray diffraction analysis of complex **55** confirmed that the macrocyclic ring exhibited only minimal distortion compared to the metal-free macrocycle, a finding ascribed to steric interactions between the exocyclic ester groups as opposed to metal coordination *per se* (Fig. 31b).[89] Relative to the other hexadentate macrocycles (e.g., amethyrin and isoamethyrin), the naphthobipyrrole unit is expected to impart greater rigidity to the macrocycle. A more planar conformation is seen upon uranyl coordination that was thought to result in a 0.431 Å reduction in the central core diameter and stronger interactions between the uranyl cation bound and the nitrogen centres present in this particular hexadentate ligand relative to its less-rigid congeners.
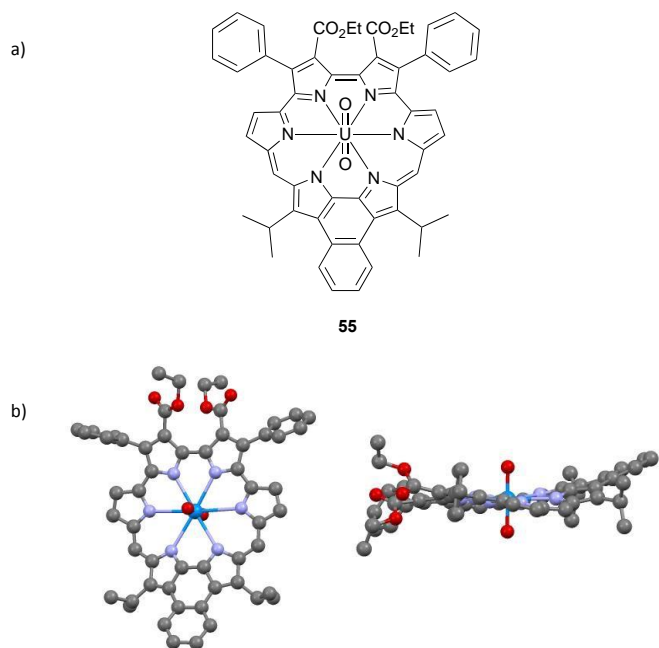
a)

55

b)

Fig. 31. A) Chemical structure of complex **55** B) Top and side views of the crystal structure of complex **55**. This figure was generated using data downloaded from the Cambridge Crystallographic Data Centre (CSD No. 1538502) as originally reported in Ref. 90.

Pyriamethyrin and dipyriamethyrin actinide complexes

Hexaphyrins containing heterocyclic subunits other than solely pyrrole are known. One set of such macrocycles, studied by Sessler and co-workers, is pyrihexaphyrin(0.1.0.0.1.0), or pyriramethyrin. This system contains a pyridine in lieu of a pyrrole. Its resemblance to amethyrin provided an inspiration to test whether it would act as an effective ligand for selected actinide cations. In fact, reaction of pyrihexaphyrin with uranyl silylamide (UO$_2$[N(SiMe$_3$)$_2$]$_2$) induced ring contraction to give the pyrihexaphyrin(0.0.0.0.1.0) complex **56** (Fig. 32a).[90] A single-crystal X-ray diffraction analysis of **56** confirmed the contraction and uranyl cation insertion into the resulting macrocycle (Fig. 32b).

It was proposed that activation of one of the *meso*-positions occurred upon coordination of the uranyl cation into the macrocycle cavity to form a 22 π-electron aromatic core as inferred from NMR spectroscopic studies. Computational analyses led to the suggestion that coordination of the uranium(VI) cation facilitated an intramolecular ring oxidation and the formation of a uranium(IV) complex, which re-oxidized to uranium(VI) when exposed to air. This proposed activated metallo-expanded porphyrin then rapidly undergoes hydroxyl nucleophilic addition into the *meso*-position followed by a rearrangement to yield the *exo*-carbaldehyde. This structure is stabilized by the uranyl centre acting as an electron sink and facilitating the final fragmentation giving rise to the oxidized aromatic product.[90]
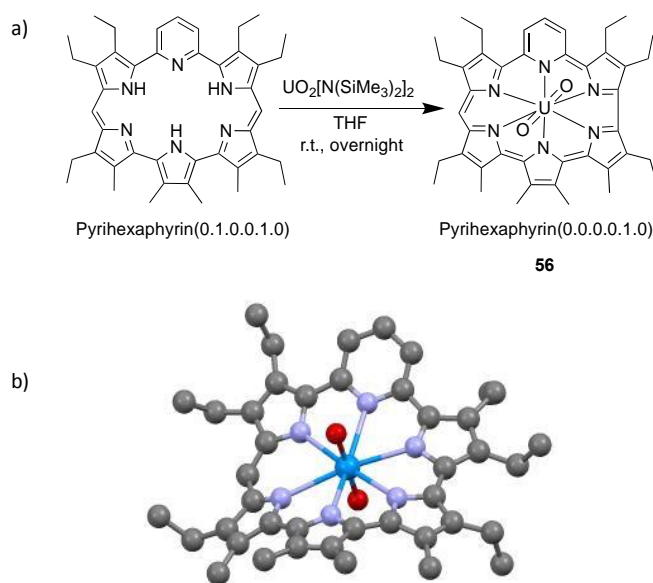
a)

Pyrihexaphyrin(0.1.0.0.1.0)   Pyrihexaphyrin(0.0.0.0.1.0)

56

b)

Fig. 32. A) Synthesis of complex **56**. Single-crystal X-ray structure of the uranyl compound **56**. Solvent molecules were omitted for clarity. This figure was generated using data downloaded from the Cambridge Crystallographic Data Centre (CSD No. 1893883) as originally reported in Ref. 91.

Another amethyrin-like macrocycle, dipyriamethyrin, which contains two pyridine subunits, has been studied as a ligand for the actinide cations. It was found to stabilize compounds containing formal U(VI), U(IV), Th(IV), and Np(IV) centers.[91,92] Initial studies involving the use of [UO$_2$[N(SiMe$_3$)$_2$]$_2$] and UO$_2$(OAc)$_2$·2H$_2$O as the uranyl cation sources and two different dipyriamethyrins allowed isolation of the corresponding uranyl complexes **57** and **58** in high yields (80 and 72%, respectively), as dark purple solids (Fig. 33a).[92] Competition experiment employing several lanthanide (e.g., LaX$_3$, GdX$_3$, NdX$_3$, TbX$_3$, and DyX$_3$; X = OAc; in CH$_2$Cl$_2$:MeOH, 1:1, v/v) or transition metal salts in the presence of a uranyl cation source yielded the uranyl complexes albeit in low yield. In analogy to what was observed with the amethyrin uranyl complex, the colours of **57** and **58** differed dramatically from those of the initial ligand form. Specifically, a change from red-orange to dark purple was seen upon uranyl cation coordination. A single-crystal X-ray diffraction analysis of **58** revealed a macrocyclic framework that was distorted, presumably to accommodate the uranyl cation within the cavity (Fig. 33b).[92]

a)   b)

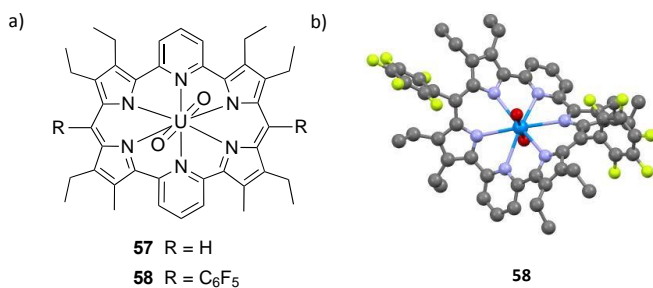**57** R = H
58 R = C$_6$F$_5$

58

Fig. 33. A) Chemical structure of the dipyriamethyrin uranyl complexes **57** and **58**. B) Single-crystal X-ray structure of compound **58**. This figure was generated using data downloaded from the Cambridge Crystallographic Data Centre (CSD No.1534774) as originally reported in Ref. 93.

The ability to coordinate the uranyl cation effectively led the Sessler group, in collaboration with the Gaunt and Arnold groups, to explore whether dipyriamethyrin would prove effective at complexing the mid-valent actinides U(IV), Th(IV), and Np(IV).[91] In fact, complexes containing these cations, structures **59–63**, could be obtained by reaction of the deprotonated dipyriamethyrin with the appropriate actinide(IV) salt, followed by treatment with sodium trimethylsilanolate in the case of complexes **62** and **63** (Fig. 34). As with the uranyl complexes **57** and **58**, distinctive colour changes, specifically from red-orange to purple-pink and light pink, were observed upon metal insertion. These complexes were characterized by Soret-like absorptions at around 482–568 nm in THF.[91] In the case of complex **62**, two additional absorptions at 531 and 577 nm were observed. These latter peaks were attributed to metal-to-ligand charge transfer (MLCT) transitions between the $5f^3$ orbitals of Np(IV) and the vacant dipyriamethyrin π^* orbital.
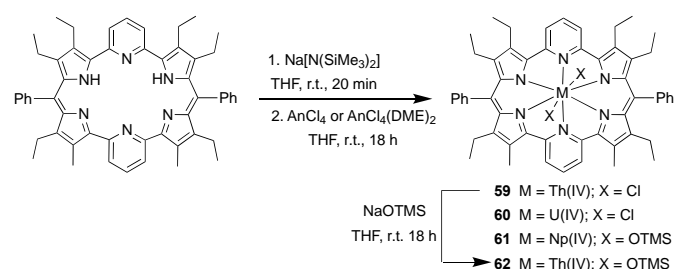

Fig. 34. Synthesis of the dipyriamethyrin actinide complexes **59–62**.

The larger cavity of dipyriamethyrin was found to accommodate the mid-valent actinide cations, U(IV), Th(IV), and Np(IV). This stands in contrast to what was observed for the Th(IV) and U(IV) porphyrin complexes discussed above. This ability to stabilize a 1:1 in-plane coordination mode was confirmed via single crystal X-ray diffraction analyses of complexes **59–62**. The resulting structures revealed six-coordinate metal centres in asymmetric tricapped geometries, as shown in Fig. 35.[91] Compared with the characteristic saddle-like structure of the free ligand, actinide cation insertion resulted in a more planar structure. This structural reorganization is thought to allow for orbital overlap between the metal cation and the coordinating aza moieties. The extent of this overlap was noted as being metal-dependent. For instance, complex **60** (containing occupied $5f^2$ orbitals), exhibited nearly linear N_{pyr}–An–N_{pyr} bond angles of 175.94 and 172.82°. A similar angle (174.21°) was seen for **61** (also containing occupied $5f^3$ orbitals). In contrast, the analogous angle is 147.19° in the case of the $5f^0$ Th(IV) complex **59**.[91] The observed angles led to the suggestion the extent of ligand–metal bonding covalency increases with increasing atomic number (i.e., Th(IV) < U(IV) < Np(IV)). This was attributed to enhanced orbital overlap between the 5f orbitals and the porphyrinoid ring orbitals as this portion of the actinide series is traversed.
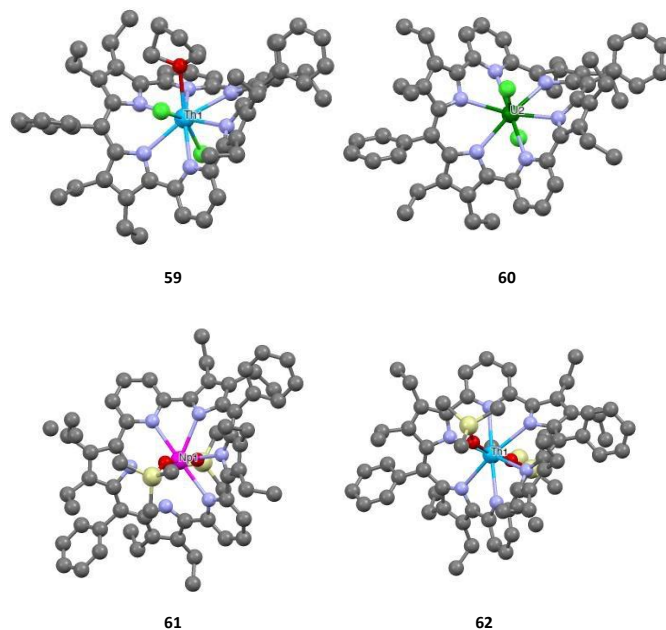

Fig. 35. Single-crystal X-ray structures of complexes **59–62**. Solvent molecules were omitted for clarity. This figure was generated using data downloaded from the Cambridge Crystallographic Data Centre (CSD No.1938484, 1901594, 1938485, and 1938486) as originally reported in Ref. 92.

Cyclo[6]pyrrole and cyclo[m]pyridine[n]pyrroles

Cyclo[n]pyrroles and cyclo[m]pyridine[n]pyrroles are macrocycles that share several attributes with other expanded porphyrins, such as larger cavities than classic tetrapyrroles, (e.g., porphyrins), an ability to coordinate larger metal cations, extended conjugation, diverse redox chemistry, and absorptions in the near-infrared region of the electromagnetic spectrum. As a result, these macrocycles have also been explored as ligands for the actinides. In fact, this series of macrocycles containing six Lewis basic donors has been found capable of supporting coordination complexes of thorium and uranium, as well as neptunium as detailed below.

Cyclo[6]pyrrole

Cyclo[n]pyrroles, first reported by Seidel *et al.*, are expanded porphyrins containing no *meso* bridges.[93] In 2003, Köhler *et al.* reported that the iron(III)-mediated cyclization of tetraalkylbipyrroles under acidic conditions produced several cyclo[n]pyrroles (n = 8, 7, and 6).[94] In particular, cyclo[6]pyrrole was found to coordinate the uranyl cation to form complex **63** (Fig. 36).[95] Formation of the uranyl complex was characterized by two-electron oxidation of the initial aromatic macrocycle (22 π-electron periphery) to form a highly stable 20 π-electron formally antiaromatic heteroannulene. The UV-vis spectrum of **63** was characterized by extinction coefficients lower than the free ligand and Soret bands at 387 and 439 nm. Complex **63** exhibited a Q-like band that was shifted to higher energy (λ_{max} = 649 nm) than the free ligand (λ_{max} = 849 nm), a difference attributed to the ligand oxidation that occurred concurrent with metal insertion. The ^{1}H NMR spectrum of **63** recorded in deuterated dichloromethane also revealed dramatic upfield shifts in the signals, a finding

rationalized in terms of a change in the ring current of the macrocycle. A single-crystal X-ray diffraction analysis of **63** revealed a six-coordinate metal centre within the macrocycle cavity giving a near-planar complex, as shown in Fig. 37.[95] The lack of *meso*-carbon bridges in the macrocycle may also contribute to the observed relatively planar geometry of the complex.
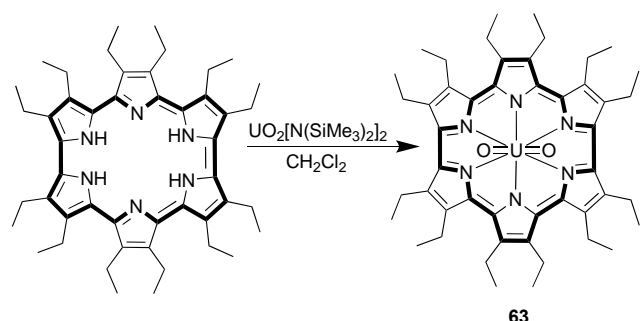

Fig. 36. Synthesis of complex **63** showing the two-electron oxidation from a 22 π-electron aromatic macrocycle to a 20 π-electron formally antiaromatic uranyl complex that occurs upon metalation.
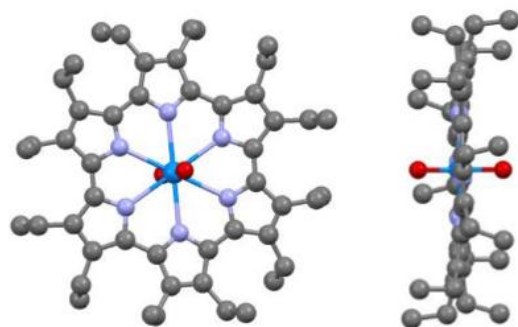

Fig. 37. Top and side views of the X-ray crystal structure of complex **63**. This figure was generated using data downloaded from the Cambridge Crystallographic Data Centre (CSD No. 641334) as originally reported in Ref. 96.

Cyclo[m]pyridine[n]pyrrole

Inspired by complex **63**, Zhang, Sessler, and co-workers prepared two hexaaza hybrid cyclo[m]pyridine[n]pyrrole macrocycles, cyclo[2]pyridine[4]pyrrole, and cyclo[3]pyridine[3]pyrrole.[96] These macrocycles displayed interesting redox properties that could be tuned through protonation. However, efforts to obtain uranyl cation complexes of these macrocycles proved unsuccessful. In contrast, an analogue of these cyclo[m]pyridine[n]pyrroles, namely cyclo[1]furan[1]pyridine[4]pyrrole, isolated via Suzuki coupling of the appropriate precursors, proved capable of stabilizing a uranyl complex (**65**; Fig. 38). Based on the optical changes accompanying metal insertion, specifically a dramatic change in colour from yellow to green, it was inferred that the system switched from a form characterized by an absence of long-range conjugation to one with aromatic character (Fig. 38).[97] This proposed conversion is analogous to what was seen in the case of complex **63** and gave rise to a distinctive UV-vis absorption spectrum. Two sharp Soret-like bands at 389 and 486 nm were seen along with three Q-like bands at 681, 847,

and 1177 nm, respectively. Furthermore, computational studies combined with a single-crystal X-ray diffraction analysis led the authors to suggest that complexation of the uranyl cation (to produce **64**) produces the inferred change in electronic configuration, which accounts for the evolution of the colour and the corresponding UV-visible spectral differences.[97] Complex **64** thus highlights how actinide cation coordination may be used to adjust the electronic features of appropriately chosen expanded porphyrin.
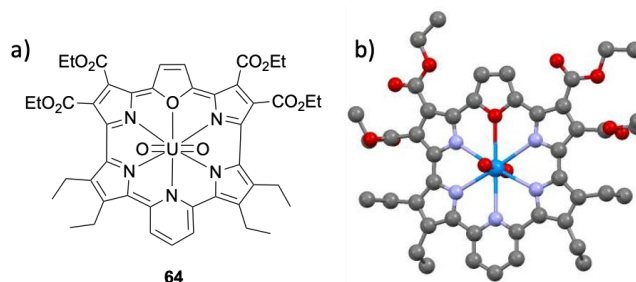

Fig. 38. a) Chemical structure of complex **64**. b) -X-ray crystal structure of complex **64**. This figure was generated using data downloaded from the Cambridge Crystallographic Data Centre (CSD No. 973875) as originally reported in Ref. 98.

Theoretical predictions and comparisons of porphyrinoid actinide complexes

Computational methods have played a critical role in the development of actinide coordination chemistry. They have helped rationalize experimental findings and have provided critical insights into fundamental questions, including the extent to which of covalency stabilizes actinide-ligand bonds. Theory has also played a critical predictive role, which has proved of particular utility in a field where highly radioactive elements are often involved. However, the high atomic number of actinides and the presence of relativistic effects has made theoretical studies of actinide complexes challenging.[98–101] As a consequence, it been necessary to strike a balance between simplification to reduce computational cost and accuracy to model the system with fidelity.

In 2008 an important study was published by Shamov and Schreckenbach that underscored the tension between computational simplicity and modeling accuracy.[102] These researchers carried out theoretical calculations on various substituted uranyl-isoamethyrin complexes and found that the simplification of the isoamethyrin (**66**) structure by removing the peripheral alkyl substituents resulted in an over-estimation of the U–N bond lengths and failed to replicate accurately the overall experimental geometry of the molecule (Fig. 39). Converting seemingly benign moieties, such as alkyl groups, to hydrogen is a commonly used approach since it reduces the computational burden. However, the authors of this study found that the steric strain induced by adjacent alkyl groups, has a large effect on the planarity of the macrocycle, which in turns shortens the U–N bond. Moreover, replacing the alkyl groups by hydrogen atoms, in this instance and others, can result in a planar aromatic macrocycle. This is seen, for instance, in the computationally simplified structure of

isoamethyrin (**66**), which adopts a planar structure in contrast to the "bent" geometry seen for the as-synthesized alkyl-substituted isoamethyrin (**65**).[86] This difference serves to highlight the caveat that theoretical simplifications of expanded porphyrin structures is a non-trivial process that can have profound effects on the accuracy of the calculations.
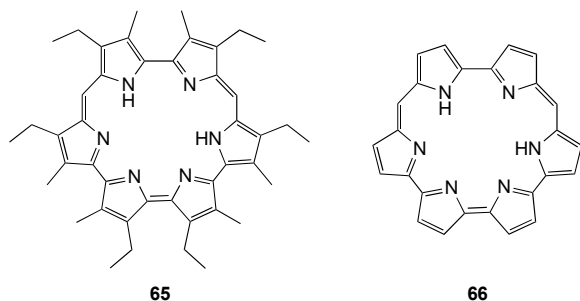

Fig. 39. Experimentally synthesized isoamethyrin **65** and simplified version **66** used in initial computational studies.

Another noteworthy theoretical study was carried out on the uranyl sapphyrin derivative (**67**),[103] analogous to complex **46** originally reported by the Sessler group in 1991.[57] In the original report, the Sessler group found that heating a mixture of free sapphyrin, methanol, and pyridine/triethylamine returned the macrocycle unchanged. However, as discussed in the section of saphhyrin and oxasapphyrin, addition of a uranyl salt led not only to metalation but as well as the formal addition of a methoxide nucleophile into one *meso*-carbon bridge of the sapphyrin core to produce an unexpected methoxide-substituted uranyl-sapphyrin complex (**46**).
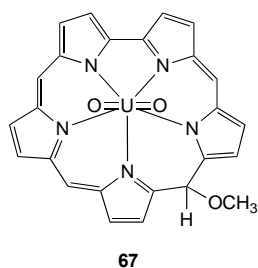

Fig. 40. Methoxide substituted uranyl-sapphyrin derivative **67** studied as a simplified model of what was observed experimentally. See structure **46**.

To probe this seemingly unusual reactivity, Shamov carried out an extensive theoretical study analysing the thermodynamic of the reaction and suggesting possible mechanistic pathways. It was found computationally that changes to the size of the inner cavity caused by the introduction of a tetrahedral carbon at the meso-bridge resulting from methoxy group incorporation increases the binding energy for uranyl cation complexation. This increase in metal-ligand bond energetics serves to overcome any energetic reduction associated with loss of aromaticity. Shamov noted that the failure of the uranyl cation to form a 1:1 complex with the unmodified sapphyrin core could be ascribed to the trianionic nature of the ligand; the uranyl complex will either have an overall charge that could not be stabilized in the solid state (at least not with the

counterion present in original experimental work) or a residual NH proton would be present in the macrocyclic core that would result in unfavourable metal-ligand interactions.

More recently (2019), the Sessler group developed a mixed hexaphyrin, pyrihexaphyrin(0.1.0.0.1.0), that undergoes ring contraction concurrent with metalation upon exposure to an appropriately chosen uranyl salt (Fig. 30).[90][68] A combination of experimental and computational methods were used to investigate the cause of this contraction. It was postulated that the addition of a hydroxide anion into the *meso*-carbon position gave a non-aromatic intermediate. However, unlike the methoxide-substituted uranyl-sapphyrin complex mentioned above, this intermediate then undergoes a ring contraction to yield the pyrihexaphyrin (0.0.0.0.1.0)-uranyl complex (**54**). The authors carried out a series of calculations to probe the aromaticity of these compounds. One part of this study relied on the use of nucleus independent chemical shift (NICS) calculations, a technique that is commonly used to measure the response of an aromatic system to an external field.[104] A second approach involved determining the anisotropy of the induced current density (ACID); this is a theoretical tool that has been used to probe electron delocalization within molecules.[105,106] Both methods have been used extensively to study the aromaticity of porphyrinoids. On the basis of ACID plots and NICS calculations, the authors suggested that the putative metalated intermediate produced upon reaction of pyrihexaphyrin(0.1.0.0.1.0) with the uranyl cation is non-aromatic. This relatively destabilized, *meso*-activated complex then undergoes hydroxide anion addition, a process that ultimately leads to ring contraction to yield the aromatic 22 π-electron Hückel-type aromatic core. In this case both aromatization and metal complexation contribute to making the reaction thermodynamically favoured.

In recent years, significant interest in the actinide-porphyrin community has been devoted to probing the nature of the actinide-ligand bond, specifically the extent of its covalency. The quantum theory of atoms in molecules (QTAIM), first introduced by Richard Bader,[107] has proven to be a valuable tool for probing covalency. QTAIM is a tool that allows one to study the topology of the electron density and thus gain insight into the bonding arrangements. One of the first reports of QTAIM applied to porphyrinoid-actinide bonding was published in 2016 by the Kerridge group. These researchers investigated the coordination chemistry of UO_2^{2+} using isoamethyrin and bis-triazinyl-pyridine (BTP) as representative ligands.[87] One key metric derived from QTAIM, the electron density at the bond critical point (BCP) ρ, provides a measure of the covalent versus ionic bond trade off. Values greater than 0.2 a.u. indicate a more covalent type of bond, while values less than 0.2 a.u. indicate bonds that are more ionic in nature. Kerridge and collaborators found that the electron density at the BCP for the U–N bonds in the uranyl-isoamethyrin complex were characterized by ρ values in the 0.026 − 0.052 a.u. range, leading to suggesting that the bonding is largely ionic in nature. On the other hand, the U–O bonds were found to have ρ values between 0.299 and 0.307 a.u., consistent with bonds that are more covalent bond in

ARTICLE

nature. As a general rule, it was found that shorter U-N bonds were correlated with larger values of ρ, supporting the intuitive view that shorter, stronger bonds, exhibit higher covalency. This led to the suggestion that the U-N bonds were primarily ionic by nature, while the U-O bonds were more covalent.

In 2019 Sessler and collaborators reported a series of dipyriamethyrin- thorium(IV), uranium(IV), uranium(VI), and neptunium(IV) complexes. The congruent nature of these complexes allowed for a direct comparison of the actinide-ligand bonding in these complexes.[91] Using several QTAIM metrics (e.g., bond critical point, change in metal spin density, and energy density) the authors concluded that traversing the An(IV)[dipyriamethyrin]Cl$_2$ series from thorium(IV) to neptunium(IV) leads to an increase in the covalent nature of the actinide-ligand bond. Orbital analysis indicated the N–Th(IV) σ-bond had little metal contribution (5.2%), as would be expected for a complex stabilized predominately via ionic interactions. In contrast, the N–U(IV) and N–Np(IV) σ-bonds had increased degrees of covalency, namely 8.3% and 11.1%, respectively. Both the uranium(IV) and the neptunium(IV) were found to interact with the ligand via the 5f-orbitals, while the bonding in the case of the thorium(IV) was primarily based on 6d orbital interactions. The authors also noted a degree of π-orbital overlap between the pyridine moieties and the coordinated actinide cations in both the uranium(IV) and neptunium(IV) complexes. Such interactions are notably absent in the case of the corresponding thorium(IV) and uranium(VI) complexes. The authors used ACID plots as an aid to visualizing the extent of covalency in the metal-ligand binding. This representation revealed electron delocalization between the pyridinyl moieties of the ligand and the metal centres in the uranium(IV) and N(IV) complexes, whereas no appreciable electron density was seen in the case of the uranyl(VI) and thorium(IV) complexes. These results led the authors to conclude that the neptunium(IV) and uranium(IV) valence electrons contribute to a delocalized metal-ligand bond between the pyridine and the metal centres, possibly through back bonding-type electron sharing.
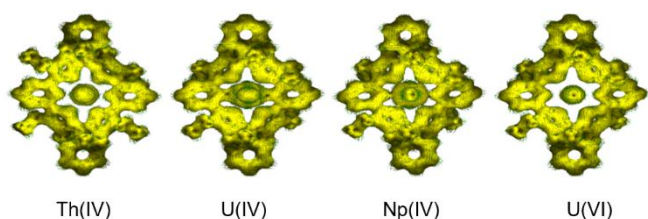

Fig. 41 ACID plots of Th(IV)(dipyriamethyrin)Cl2, U(VI)O2(dipyriamethyrin), U(IV)(dipyriamethyrin)Cl2, and Np(IV)(dipyriamethyrin)Cl2, showing the extent of π-electron delocalization between the dipyriamethyrin ligand and the actinide ion. Reprinted with permission from ref. 69. Copyright 2019 American Chemical Society.

Recently, Yang *et al.* investigated the electronic and coordinative properties of AnO$_2^{2+/+}$ in a series of expanded

porphyrins amethyrin, oxasapphyrin, and grandephyrin.[108] Using natural population analysis and QTAIM techniques they were able to calculate the binding free energy in MeOH and found that PuO$_2^{2+}$ and NpO$_2^{2+}$ ions displayed the strongest binding affinities amongst the series consisting of UO$_2^{2+}$, UO$_2^+$, NpO$_2^+$, and PuO$_2^+$ for each of the ligands, with the bonding being predominantly ionic. These researchers also found that oxasapphyrin displays a greater binding affinity than either amethyrin or grandephyrin. This is consistent with the suggestion that the replacement of pyrrole by furan favours actinyl cation complexation.

Recently, computational chemistry has emerged as a predictor that can guide the direction of f-element research. For instance, in a recent paper Schreckenbach *et al.* explored the possibility of different actinyl ions complexing with dipyriamethyrin.[109] While the Sessler group had previously reported the synthesis of the An(IV) and U(VI) dipyriamethyrin complexes, Schreckenbach used natural population analysis to show that the pyrrole nitrogen atoms in all complexes carried greater negative charges than the pyrroline nitrogen atoms. This led to the suggestion that metal complexation is dominated by interactions with the pyrrolic nitrogen atoms. Calculated formation energies for the actinyl (VI,V) complexes in both the gas phase and in dichloromethane solution were found to decrease in the order UO$_2$L>PuO$_2$L>NpO$_2$L>AmO$_2$L, where L = dipyriamethyrin). The calculated ΔG and ΔH values were negative for all complexes, leading to the prediction that these complexes could potentially be synthesized. Using energy decomposition analysis, these researchers found that although the actinyl(V/VI) ligand bonding interactions were predominantly electrostatic in nature, some covalency did persist that was expected to decrease gradually from U to Am. This was found for both the pentavalent and hexavalent actinyl complexes, leading to the suggestion that these complexes would prove stable. Computational methods have thus have not only helped us explain current experimental findings, but are also providing a light that is expected to help guide future research.

Conclusions

In conclusion, the coordination chemistry of actinide cations with porphyrinoid ligands has been of great interest for more than 70 years. Although most of the complexes studied to date contain early actinides, some examples with transuranic metals have been reported. The high coordination number of actinide metal cations has led to the synthesis of porphyrinoid complexes with diverse architectures, including double- and triple-decker structures, dimers, and trimers. In this sense, porphyrinoids as ligands have allowed explorations of metal-ligand interactions and also advanced our fundamental understanding of the coordination chemistry of the actinide cations, work that provides an intellectual foundation for exploiting these complexes in different fields, such as for nuclear energy industry or waste remediation. Included in this latter area are the limited, but increasing, number of studies focused on the use of expanded porphyrins as ligands for

transuranic cations or to stabilize complexes of less-common oxidation states of the early actinide elements (e.g., U(IV)). The work carried out so far has allowed insights into how certain oxidation states of actinide cations are better accommodated by a given porphyrinoid ligand or how the ligand frameworks may adjust their electronic features to accommodate a specific actinide cation. This progress, combined with the importance of understanding the chemistry of actinide cations, provides an incentive to explore further the actinide coordination chemistry of novel oligopyrrolic ligands. It is hoped that the present review will provide a foundation for future research efforts along these lines.

Author Contributions

All authors contributed to the writing and proof reading of this manuscript.

Conflicts of interest

There are no conflicts to declare.

Acknowledgements

Notes and references

‡ These values were measured using Mercury 3.10.3 version using data downloaded from the Cambridge Crystallographic Data Centre (CSD No 1938306) as originally reported in Ref. 40.

Biographies:

From left to right: Daniel Mangel, Dr. Gabriela I. Vargas-Zúñiga & Prof. Jonathan L. Sessler

Jonathan L. Sessler received a BSc degree in Chemistry in 1977 from the University of California, Berkeley and a PhD from Stanford University in 1982. After postdoctoral stays in Strasbourg and Kyoto, he accepted a position as an Assistant Professor of Chemistry at The University of Texas at Austin, where he is the Doherty-Welch Chair. He has held a number of visiting professorships, including most recently (from September 2015-August 2020) at Shanghai University. He was a co-founder of Pharmacyclics, Inc. and OncoTEX, Inc. In April of 2021 he was elected to the U.S. National Academy of Sciences.

Gabriela I. Vargas-Zúñiga received her B.Sc. and M.Sc. in Chemistry from the National Autonomous University of Mexico, Mexico City. She earned her Ph.D. degree from the University of Texas at Austin in 2013 under the supervision of Prof. Jonathan L. Sessler. She is currently a research associate in the same group. Her research interests include synthetic anion and ion pair receptors, and polypyrrole-based actinide coordination chemistry.

Daniel N. Mangel received his B.A. and M. Sc. in chemistry from Concordia University, Montreal, Canada where he performed research with Prof. Pat Forgione in the field of organometallic chemistry. Daniel then moved to The University of Texas at Austin where he is currently pursuing a Ph.D. under the supervision of Prof. Jonathan L. Sessler. His research revolves exploring expanded porphyrins and their coordination to actinide and lanthanide cations using both computational and experimental methods.

Dr. Michael A. Boreen (left) and Prof. John Arnold (right)

Michael A. Boreen graduated in 2015 with a B.A. in Chemistry and Biochemistry and a M.S. in Chemistry from the Vagelos Scholars Program in the Molecular Life Sciences at the University of Pennsylvania where he performed research with Professor Eric Schelter. He earned his Ph.D. in Chemistry in 2020 from the University of California, Berkeley under the supervision of Professor John Arnold, specializing in strong bond activation and small molecule reactivity with low-valent uranium complexes. He is currently a postdoctoral researcher in the groups of Professors Alexander Katz and John Arnold at UC Berkeley, focusing on designing supported molecular catalysts.

John Arnold is a Professor of Chemistry and Undergraduate Dean in the College of Chemistry at UC Berkeley. He is a graduate of the University of Salford (Applied Chemistry, 1982) and the University of California, San Diego (Ph.D. 1986). He carried out postdoctoral work with Professor Sir Geoffrey Wilkinson at Imperial College, London from 1987-88, before a short stint as a Royal Society University Research Fellow (1988-89). He began his independent career at UC Berkeley as an Assistant Professor in 1989.

Abbreviations:

1-ClN	1-chloronaphthaline
acac	acetylacetonate
AcOH	acetic acid
ACID	anisotropy of the induced current density
DME	dimethoxyethane
DMF	dimethylformamide
HOMO	highest occupied molecular orbital
LUMO	lowest unoccupied molecular orbital
MeOH	methanol
MLCT	metal-to-ligand charge transfer
OAc	acetate
OEP	octaethylporphyrin
Pc	phthalocyanine
PhCN	benzonitrile
QTAIM	quantum theory of atoms in molecules
SPc	superphthalocyanine
THF	tetrahydrofuran
TPP	tetraphenylporphyrin
TpTP	tetra-*p*-tolylporphyrin

Notes and references

1   H. H. Dam, D. N. Reinhoudt and W. Verboom, *Chem. Soc. Rev.*, 2007, **36**, 367–377.

2   J. H. Lan, W. Q. Shi, L. Y. Yuan, J. Li, Y. L. Zhao and Z. F. Chai, *Coord. Chem. Rev.*, 2012, **256**, 1406–1417.

3   L. E. Roy, N. J. Bridges and L. R. Martin, *J. Chem. Soc. Dalt. Trans.*, 2013, **42**, 2636–2642.

4   J. C. Gordon, K. Czerwinski and L. Francesconi, *Inorg. Chem.*, 2013, **52**, 3405–3406.

5   J. E. Bloor, J. Schlabitz, C. C. Walden and A. Demerdache, *Can. J. Chem.*, 1964, **42**, 2201–2208.

6   F. Lux and F. Ammentorp-Schmidt, *Radiochim. Acta*, 1965, **4**, 112–113.

7   V. F. Lux, D. Dempf and D. Graw, *Angew. Chem.*, 1968, **80**, 792–793.

8   F. Lux, D. Dempf and D. Graw, *Angew. Chem. Int. Ed. Engl.*, 1968, **7**, 819–820.

9   T. J. Marks and D. R. Stojakovic, *J. Chem. Soc. Chem. Commun.*, 1975, 28–29.

10   T. J. Marks and D. R. Stojakovic, *J. Am. Chem. Soc.*, 1978, **100**, 1695–1705.

11   E. A. Cuellar and T. J. Marks, *Inorg. Chem.*, 1981, **20**, 3766–3770.

12   V. W. Day, T. J. Marks and W. A. Wachter, *J. Am. Chem. Soc.*, 1975, **97**, 4519–4527.

13   F. Lux, F. Ammentorp-Schmidt, D. Dempf, D. Graw and W. Hagenberg, *Radiochim. Acta*, 1970, **14**, 57–61.

14   J. L. Sessler and S. J. Weghorn, *Expanded, Contracted & Isomeric Porphyrins*, Pergamon, First., 1997.

15   J. T. Brewster, H. Zafar, H. D. Root, G. D. Thiabaud and J. L. Sessler, *Inorg. Chem.*, 2020, **59**, 32–47.

16   R. P. Linstead, *J. Chem. Soc.*, 1934, 1016–1017.

17   S. Yamamoto, S. V. Dudkin, M. Kimura and N. Kobayashi, in *Handbook of Porphyrin Science*, World Scientific, 2019, pp. 1–168.

18   F. H. Moser and A. L. Thomas, *The phthalocyanines*, CRC Press, Boca Raton, Fla, 1983.

19   A. B. Sorokin, *Chem. Rev.*, 2013, **113**, 8152–8191.

20   D. Gounden, N. Nombona and W. E. van Zyl, *Coord. Chem. Rev.*, 2020, **420**, 213359.

21   M. Urbani, M.-E. Ragoussi, M. K. Nazeeruddin and T. Torres, *Coord. Chem. Rev.*, 2019, **381**, 1–64.

22   K. A. Hahn, M. Panjehpour and X. Lu, *Photochem. Photobiol.*, 1996, **63**, 117–122.

23   Y. Zhang and J. F. Lovell, *WIREs Nanomed Nanobiotechnol*, 2017, **9**, e1420.

24   P. Vasudevan, S. Neelam, N. Mann and S. Tyagi, *Transit. Met. Chem.*, 1990, 15, 81–90.

25   G. Bottari, G. de la Torre, D. M. Guldi and T. Torres, *Chem. Rev.*, 2010, **110**, 6768–6816.

26   G. Guillaud, J. Simon and J. P. Germain, *Coord. Chem. Rev.*, 1998, 178–180, 1433–1484.

27   K. P. Ng and J. Jiang, *Chem. Soc. Rev.*, 1997, 26, 433–442.

28   K. M. Kadish, G. Moninot, Y. Hu, D. Dubois, A. Ibnlfassi, J. M. Barbe and R. Guilard, *J. Am. Chem. Soc.*, 1993, **115**, 8153–8166.

29   T. N. Lomova, M. E. Klyueva and O. I. Koifman, *Macroheterocycles*, 2015, **8**, 32–46.

30   P. N. Moskalev, G. N. Shapkin and A. N. Z. Darovskih, *Neorg. Khim.*, 1979, **24**, 340–346.

31   C. Harnoode, K. Takamura, H. Kubota, K. Sho, K. Fijusawa, F. Kitamura, T. Ohsaka and K. Tokuda, *Electrochemistry*, 1999, **67**, 832–838.

32   J. Janczak and R. Kubiak, *Polyhedron*, 1999, **18**, 1621–1627.

33   J. Janczak, R. Kubiak, I. Svoboda, A. Jezierski and H. Fuess, *Inorganica Chim. Acta*, 2000, **304**, 150–155.

34   A. Capobianchi, C. Ercolani, A. M. Paoletti, G. Pennesi, G. Rossi, A. Chiesi-Villa and C. Rizzoli, *Inorg. Chem.*, 1993, **32**, 4605–4611.

35   J. Janczak, R. Kubiak and F. Hahn, *Inorg. Chim. Acta*, 1998, **281**, 195–200.

36   M. Haghighi, M. Safarpour Rath, H. W. Rotter and Z. Homborg, H., *Anorg. Allg. Chem.*, 1993, **619**, 1887–1896.

37   G. Ostendorp, H. W. Rotter and H. Homborg, *Zeitschrift fur Naturforsch. B*, 1996, **51**, 567–573.

38   A. Dormond, B. Belkalem, R. Guilard, P. Charpin, M. Lance, D. Vigner and G. Folcher, *Inorg. Chem.*, 1986, **25**, 4785–4790.

39   R. Guilard, A. Dormond, M. Belkalem, J. E. Anderson, Y. H.

Liu and K. M. Kadish, *Inorg. Chem.*, 1987, **26**, 1410–1414.

40 W. Zhou, D. McKearney and D. B. Leznoff, *Chem. - A Eur. J.*, 2020, **26**, 1027–1031.

41 G. S. Girolami, S. N. Milam and K. S. Suslick, *Inorg. Chem.*, 1987, **26**, 343–344.

42 W. Zhou, R. H. Platel, T. Teixeira Tasso, T. Furuyama, N. Kobayashi and D. B. Leznoff, *Dalt. Trans.*, 2015, **44**, 13955–13961.

43 E. W. Y. Wong, C. J. Walsby, T. Storr and D. B. Leznoff, *Inorg. Chem.*, 2010, **49**, 3343–3350.

44 A. A. Ptaszyńska, M. Trytek, G. Borsuk, K. Buczek, K. Rybicka-Jasińska and D. Gryko, *Sci. Rep.*, 2018, **8**, 5523.

45 G. Varchi, F. Foglietta, R. Canaparo, M. Ballestri, F. Arena, G. Sotgiu, A. Guerrini, C. Nanni, G. Cicoria, G. Cravotto, S. Fanti and L. Serpe, *Nanomedicine*, 2015, **10**, 3483–3494.

46 G. de la Torre, G. Bottari, M. Sekita, A. Hausmann, D. M. Guldi and T. Torres, *Chem. Soc. Rev.*, 2013, **42**, 8049–8105.

47 C.-P. Wong and W. D. Horrocks, *Tetrahedron Lett.*, 1975, 2637–2640.

48 G. Knör and A. Strasser, *Inorg. Chem. Commun.*, 2002, **5**, 993–995.

49 M. Taniguchi, J. S. Lindsey, D. F. Bocian and D. Holten, *J. Photochem. Photobiol. C Photochem. Rev.*, 2021, **46**, 100401.

50 J.-P. Strachan, S. Gentemann, J. Seth, W. A. Kalsbeck, J. S. Lindsey, D. Holten and D. F. Bocian, *J. Am. Chem. Soc.*, 1997, **119**, 11191–11201.

51 A. Dormond, B. Belkalem and R. Guilard, *Polyhedron*, 1984, **3**, 107–112.

52 K. M. Kadish, Y. H. Liu, J. E. Anderson, P. Charpin, G. Chevrier, M. Lance, M. Nierlich, D. Vigner, A. Dormond, B. Belkalem and R. Guillard, *J. Am. Chem. Soc.*, 1988, **110**, 6455–6462.

53 T. H. Tran-Thi, A. Dormond and R. Guilard, *J. Phys. Chem.*, 1992, **96**, 3139–3145.

54 G. W. Watt and K. F. Gadd, *Inorg. Nucl. Chem. Lett.*, 1973, **9**, 203–205.

55 G. S. Girolami, S. N. Milam and K. S. Suslick, *J. Am. Chem. Soc.*, 1988, **110**, 2011–2012.

56 G. S. Girolami, P. A. Gorlin, S. N. Milam, K. S. Suslick and S. R. Wilson, *J. Coord. Chem.*, 1994, **32**, 173–212.

57 J. W. Buchler and B. Scharbert, *J. Am. Chem. Soc.*, 1988, **110**, 4272–4276.

58 R. J. Donohoe, J. K. Duchowski and D. F. Bocian, *J. Am. Chem. Soc.*, 1988, **110**, 6119–6124.

59 E. Rheinfrank, M. Pörtner, M. del C. Nuñez Beyerle, F. Haag, P. S. Deimel, F. Allegretti, K. Seufert, J. V. Barth, M.-L. Bocquet, P. Feulner and W. Auwärter, *J. Am. Chem. Soc.*, 2021, **143**, 14581–14591.

60 T. N. Lomova, L. G. Andrianova and B. D. Berezin, *Zhurnal Neorg. Khimii*, 1991, **36**, 641–646.

61 T. N. Lomova and L. G. Andrianova, *Mendeleev Commun.*, 2003, **13**, 213–214.

62 C. C. Leznoff and A. B. P. Lever, *Phthalocyanines: Properties and Applications*, VCH, New York, 1997.

63 B. Patra, S. Mondal and S. Kar, in *Encyclopedia of Inorganic and Bioinorganic Chemistry*, ed. R. A. Scott, 2022, pp. 1–24.

64 M. Stefanelli, S. Nardis, L. Tortora, F. R. Fronczek, K. M. Smith, S. Licoccia and R. Paolesse, *Chem. Commun.*, 2011, **47**, 4255–4257.

65 H. L. Buckley, W. A. Chomitz, B. Koszarna, M. Tasior, D. T. Gryko, P. J. Brothers and J. Arnold, *Chem. Commun.*, 2012, **48**, 10766–10768.

66 S. Nardis, F. Mandoj, M. Stefanelli and R. Paolesse, *Coord. Chem. Rev.*, 2019, **388**, 360–405.

67 A. L. Ward, H. L. Buckley, W. W. Lukens and J. Arnold, *J. Am. Chem. Soc.*, 2013, **135**, 13965–13971.

68 V. J. Bauer, D. L. J. Clive, D. Dolphin, J. B. Paine, F. L. Harris, M. M. King, J. Loder, S. W. C. Wang and R. B. Woodward, *J. Am. Chem. Soc.*, 1983, **105**, 6429–6436.

69 S. Saito and A. Osuka, *Angew. Chem. Int. Ed.*, 2011, **50**, 4342–4373.

70 T. Tanaka and A. Osuka, *Chem. Rev.*, 2017, **117**, 2584–2640.

71 J.-Y. Shin, K. S. Kim, M.-C. Yoon, J. M. Lim, Z. S. Yoon, A. Osuka and D. Kim, *Chem. Soc. Rev.*, 2010, **39**, 2751.

72 G. I. Vargas-Zúñiga and J. L. Sessler, *Adv. Inorg. Chem.*, 2018, **71**, 327–377.

73 T. Furuyama, Y. Ogura, K. Yoza and N. Kobayashi, *Angew. Chem. Int. Ed.*, 2012, **51**, 11110–11114.

74 S. V. Rao, N. Venkatram, L. Giribabu and D. N. Rao, *J. Appl. Phys.*, 2009, **105**, 053109.

75 M. Friedman, *J. Org. Chem.*, 1956, **30**, 859–863.

76 J. L. Sessler, A. E. Vivian, D. Seidel, A. K. Burrell, M. Hoehner, T. D. Mody, A. Gebauer, S. J. Weghorn and V. Lynch, *Coord. Chem. Rev.*, 2001, **216–217**, 411–434.

77 H. Rexhausen and A. Gossauer, *J. Chem. Soc., Chem. Commun.*, 1983, 275.

78 A. K. Burrell, G. Hemmi, V. Lynch and J. L. Sessler, *J. Am. Chem. Soc.*, 1991, **113**, 4690–4692.

79 J. L. Sessler, A. E. V Gorden, D. Seidel, S. Hannah, V. Lynch, P. L. Gordon, R. J. Donohoe, C. D. Tait and D. W. Keogh, *Inorg. Chim. Acta*, 2002, **341**, 54–70.

80 R. B. Woodward, ed. 1966 The Chemical Society: London, Sheffield, 1966.

81 A. K. Burrell, M. J. Cyr, V. Lynch and J. L. Sessler, *J. Chem. Soc. Chem. Commun.*, 1991, 1710–1713.

82 J. L. Sessler, A. Gebauer, M. C. Hoehner and V. M. Lynch, *Chem. Commun.*, 1998, 1835–1836.

83 J. L. Sessler, S. J. Weghorn, Y. Hiseada and V. Lynch, *Chem. Eur. J.*, 1995, **1**, 56–67.

84 J. L. Sessler, S. J. Weghorn, T. Morishima, M. Rosingana, V. Lynch and V. Lee, *J. Am. Chem. Soc.*, 1992, **114**, 8306–8307.

85 S. Hannah, D. Seidel, J. L. Sessler and V. Lynch, *Inorganica Chim. Acta*, 2001, **317**, 211–217.

86 J. L. Sessler, D. Seidel, A. E. Vivian, V. Lynch, B. L. Scott and D. W. Keogh, *Angew. Chem. Int. Ed.*, 2001, **40**, 591–594.

87 P. Di Pietro and A. Kerridge, *Phys Chem Chem Phys*, 2016, **18**, 16830–16839.

88 J. T. Brewster, A. Aguilar, G. Anguera, H. Zafar, M. D. Moore and J. L. Sessler, *J. Coord. Chem.*, 2018, **71**, 1808–1813.

89 G. Anguera, J. T. Brewster, M. D. Moore, J. Lee, G. I. Vargas-Zúñiga, H. Zafar, V. M. Lynch and J. L. Sessler, *Inorg. Chem.*, 2017, **56**, 9409–9412.

90   J. T. Brewster, H. D. Root, D. Mangel, A. Samia, H. Zafar, A. C. Sedgwick, V. M. Lynch and J. L. Sessler, *Chem. Sci.*, 2019, **10**, 5596–5602.

91   J. T. Brewster, D. N. Mangel, A. J. Gaunt, D. P. Saunders, H. Zafar, V. M. Lynch, M. A. Boreen, M. E. Garner, C. A. P. Goodwin, N. S. Settineri, J. Arnold and J. L. Sessler, *J. Am. Chem. Soc.*, 2019, **141**, 17867–17874.

92   J. T. Brewster, Q. He, G. Anguera, M. D. Moore, X. S. Ke, V. M. Lynch and J. L. Sessler, *Chem. Commun.*, 2017, **53**, 4981–4984.

93   D. Seidel, V. Lynch and J. L. Sessler, *Angew. Chem. Int. Ed.*, 2002, **41**, 1422–1425.

94   T. Köhler, D. Seidel, V. Lynch, F. O. Arp, Z. Ou, K. M. Kadish and J. L. Sessler, *J. Am. Chem. Soc.*, 2003, **125**, 6872–6873.

95   P. J. Melfi, K. K. Sung, T. L. Jeong, F. Bolze, D. Seidel, V. M. Lynch, J. M. Veauthier, A. J. Gaunt, M. P. Neu, Z. Ou, K. M. Kadish, S. Fukuzumi, K. Ohkubo and J. L. Sessler, *Inorg. Chem.*, 2007, **46**, 5143–5145.

96   Z. Zhang, J. M. Lim, M. Ishida, V. V. Roznyatovskiy, V. M. Lynch, H. Y. Gong, X. Yang, D. Kim and J. L. Sessler, *J. Am. Chem. Soc.*, 2012, **134**, 4076–4079.

97   I. T. Ho, Z. Zhang, M. Ishida, V. M. Lynch, W. Y. Cha, Y. M. Sung, D. Kim and J. L. Sessler, *J. Am. Chem. Soc.*, 2014, **136**, 4281–4286.

98   G. Schreckenbach and G. A. Shamov, *Acc. Chem. Res.*, 2010, **43**, 19–29.

99   D. Wang, W. F. van Gunsteren and Z. Chai, *Chem. Soc. Rev.*, 2012, **41**, 5836–5865.

100   J.-P. Dognon, *Coord. Chem. Rev.*, 2014, **266–267**, 110–122.

101   N. Kaltsoyannis, *Chem. Soc. Rev.*, 2003, **32**, 9–16.

102   G. A. Shamov and G. Schreckenbach, *Inorg. Chem.*, 2008, **47**, 805–811.

103   G. A. Shamov, *J Am Chem Soc*, 2011, **133**, 4316–4329.

104   P. von R. Schleyer, C. Maerker, A. Dransfeld, H. Jiao and N. J. R. van Eikema Hommes, *J. Am. Chem. Soc.*, 1996, **118**, 6317–6318.

105   R. Herges and D. Geuenich, *J. Phys. Chem. A*, 2001, **105**, 3214–3220.

106   D. Geuenich, K. Hess, F. Köhler and R. Herges, *Chem. Rev.*, 2005, **105**, 3758–3772.

107   R. F. W. Bader, *Atoms in Molecules: A Quantum Theory*, Oxford:Clarendon Press, 1990.

108   M. Yang and D. Wang, *New J. Chem.*, 2016, **41**, 63–74.

109   E. Varathan, Y. Gao and G. Schreckenbach, *J. Phys. Chem. A*, 2021, **125**, 920–932.